Supporting Information

Assessing the feasibility of soil-based mass balance approaches to quantify CO_2 removal from enhanced rock weathering for soils of the contiguous USA

T. Jesper Suhrhoff[1,2] and Tom Reershemius[2], Jiuyuan Wang[2], Jacob S. Jordan[3, 4], Christopher T. Reinhard[5], Noah J. Planavsky[2,1]

[1] **Yale Center for Natural Carbon Capture, Yale University, New Haven, CT 06511, USA**
[2] **Department of Earth and Planetary Sciences, Yale University, New Haven, CT 06511, USA**
[3] **Porecast Research, Lawrence, KS 66046, USA**
[4] **MATI Carbon, Houston, USA**
[4] **School of Earth & Atmospheric Sciences, Georgia Institute of Technology, Atlanta, USA**

Contents

Supporting Figures

1.1 Treatment of analytical uncertainties

Every elemental concentration measurement made is associated with an analytical uncertainty that is dependent on treatment of a sample from field through laboratory (e.g. pipetting), the type of analysis (e.g. ID-ICP-MS), the instrumentation used (e.g. quadropole vs magnetic sector ICP-MS), and treatment of data (e.g. sample-standard bracketing). This uncertainty may be reported one of several ways; most commonly; (1) the % deviation of one or multiple reference standards, measured alongside samples, from their reported values. Alternatively; (2) the standard deviation (σ) of multiple replicates of a reference standard as a % of their reported values may be used. Replicates of samples can also be measured, either (3) from the same prepared aliquot of sample, which gives a measure of uncertainty associated with instrumentation and data treatment, or (4) from a separately prepared aliquot of sample, which also includes laboratory-associated uncertainty. Analytical uncertainty is generally reported as a % of a sample concentration; as such, the same uncertainty is greater in absolute terms, the larger the concentration of a sample. This scenario is shown in Fig. S1a, in a theoretical case (where *i* is an immobile element, and *j* is a mobile element).

Analytical uncertainty pertains to a single measurement – however, uncertainty on a measured value can also be reduced by repeating single measurements on replicate samples sufficiently that a mean can be calculated for those samples with standard deviation (σ) that is smaller than analytical uncertainty. This can be applied to the bulk feedstock composition, which can be assumed as homogeneous on the scale of field deployment; thus it is likely cost-effective to repeat measurements of feedstock elemental composition. A feasible outcome when plotted in a mixing diagram is shown in Fig. S1b. Using the scenario in Fig. S1b, we can plot a theoretical mixture (c_m) that has [i] and [j] exactly halfway between the endmember concentrations. Loss of *j* due to weathering will cause this sample to plot below the mixing line (c_n). The measurement uncertainty is shown in Fig. S1c.

1.2 Full derivation of expressions for minimum resolvable feedstock application, *a*, and dissolution, *b*

We first derive an uncertainty, e^j, for the theoretical mixture, c_m:

$$e_m^j = e_s^j + (e_f^j - e_s^j) * \frac{[j]_m - [j]_s}{[j]_f - [j]_s} \quad (1)$$

The limit of resolvability for $\Delta[j]$ due to dissolution is given by the expression:

$$e_n^j + e_m^j < [j]_m - [j]_n \quad (2)$$

And therefore, substituting (1) into (2):

$$e_n^j + e_s^j + (e_f^j - e_s^j) * \frac{[j]_m - [j]_s}{[j]_f - [j]_s} < [j]_m - [j]_n \quad (3)$$

We can define *a* (mass ratio of feedstock in a mixture based on application) and *b* (the fraction of feedstock dissolved), such that the following holds:

$$a * b * [j]_f = [j]_m - [j]_n \quad (4)$$

Combining (4) and (2) – see Main Text – gives an expression for the minimum resolvable a and b given uncertainty, which we can solve with respect to either variable:

$$a * b * [j]_f > e_n^j + e_m^j \quad (5)$$

Assuming uncertainty on the soil endmember and the sample end composition (c_n) are purely analytical uncertainty of the same magnitude, meaning absolute uncertainty is dependent on concentration [j], we can relate e_n^j to e_s^j:

$$e_n^j = \frac{[j]_n}{[j]_s} * e_s^j \quad (S1)$$

This can be expressed both in terms of a and in terms of b. The expressions for $[j]_m$ and $[j]_n$ in terms of a and b are as follows:

$$[j]_m = a * [j]_f + (1 - a) * [j]_s \quad (S2)$$

$$[j]_n = (1 - a) * [j]_s + a * [j]_f * (1 - b) = (1 - a) * [j]_s + a * [j]_f - a * [j]_f * b \quad (S3)$$

Substituting for $[j]_n$ from (S3) into (S1):

$$e_n^j = \frac{(1-a)*[j]_s + a*[j]_f - a*[j]_f*b}{[j]_s} * e_s^j \quad (S4)$$

Then, substituting for e_n^j from (S4), and for e_m^j from (1), into (5):

$$a * b * [j]_f > \left(\frac{(1-a)*[j]_s + a*[j]_f - a*[j]_f*b}{[j]_s} * e_s^j\right) + \left(e_s^j + (e_f^j - e_s^j) * \frac{[j]_m - [j]_s}{[j]_f - [j]_s}\right) \quad (S5)$$

And, substituting for $[j]_m$ from (S2) into (S5):

$$a * b * [j]_f > \left(\frac{(1-a)*[j]_s + a*[j]_f - a*[j]_f*b}{[j]_s} * e_s^j\right) + \left(e_s^j + (e_f^j - e_s^j) * \frac{(a*[j]_f + (1-a)*[j]_s) - [j]_s}{[j]_f - [j]_s}\right) \quad (S6)$$

Simplifying and rearranging, this gives expressions for b and a purely in terms of $[j]_s$, $[j]_f$, e_s^j, e_f^j, and a or b respectively:

$$a * b * [j]_f > \left(\frac{[j]_s - a*[j]_s + a*[j]_f - a*[j]_f*b}{[j]_s} * e_s^j\right) + \left(e_s^j + (e_f^j - e_s^j) * \frac{(a*[j]_f + [j]_s - a*[j]_s) - [j]_s}{[j]_f - [j]_s}\right) \quad (S6.1)$$

$$a * b * [j]_f > \left(\frac{[j]_s - a*[j]_s + a*[j]_f - a*[j]_f*b}{[j]_s} * e_s^j\right) + \left(e_s^j + (e_f^j - e_s^j) * a\right) \quad (S6.2)$$

We can multiply $[j]_s$ in both sides, knowing that $[j]_s > 0$ and therefore > is not flipped:

$$a * b * [j]_f * [j]_s > ([j]_s - a * [j]_s + a * [j]_f - a * [j]_f * b) * e_s^j + (e_s^j + (e_f^j - e_s^j) * a) * [j]_s \quad (S6.3)$$

Rearranging:

$$a * b * [j]_f * [j]_s + a * b * [j]_f * e_s^j > ([j]_s - a * [j]_s + a * [j]_f) * e_s^j + (e_s^j + (e_f^j - e_s^j) * a) * [j]_s \quad \text{(S6.4)}$$

$$b * (a * [j]_f * [j]_s + a * [j]_f * e_s^j) > [j]_s * e_s^j - a * [j]_s * e_s^j + a * [j]_f * e_s^j + e_s^j * [j]_s + a * e_f^j * [j]_s - a * e_s^j * [j]_s \quad \text{(S6.5)}$$

$$b * (a * [j]_f * [j]_s + a * [j]_f * e_s^j) > 2 * e_s^j * [j]_s - 2 * a * e_s^j * [j]_s + a * [j]_f * e_s^j + a * e_f^j * [j]_s \quad \text{(S6.6)}$$

$$b * (a * [j]_f * [j]_s + a * [j]_f * e_s^j) > 2 * (1 - a) * e_s^j * [j]_s + a * ([j]_f * e_s^j + e_f^j * [j]_s) \quad \text{(S6.7)}$$

Since $(a * [j]_f * [j]_s + a * [j]_f * e_s^j) > 0$, $>$ is not flipped:

$$b > \frac{2*(1-a)*e_s^j*[j]_s + a*([j]_f*e_s^j + e_f^j*[j]_s)}{a*[j]_f*[j]_s + a*[j]_f*e_s^j} \quad \text{(S6.8)}$$

Rearranging, we derive an expression for b in terms of a:

$$b > \frac{2*\frac{(1-a)}{a}*e_s^j*[j]_s + e_s^j*[j]_f + e_f^j*[j]_s}{[j]_s*[j]_f + e_s^j*[j]_f} \quad \text{(6a)}$$

We can solve for a by rearranging (6a):

$$([j]_s * [j]_f + e_s^j * [j]_f) * b > \left(\frac{1}{a} - 1\right) * 2 * e_s^j * [j]_s + e_s^j * [j]_f + e_f^j * [j]_s \quad \text{(S6.9)}$$

$$([j]_s * [j]_f + e_s^j * [j]_f) * b - e_s^j * [j]_f + e_f^j * [j]_s > \left(\frac{1}{a} - 1\right) * 2 * e_s^j * [j]_s \quad \text{(S6.10)}$$

$$\frac{([j]_s*[j]_f + e_s^j*[j]_f)*b - e_s^j*[j]_f + e_f^j*[j]_s}{2*e_s^j*[j]_s} > \left(\frac{1}{a} - 1\right) \quad \text{(S6.11)}$$

$$\frac{([j]_s*[j]_f + e_s^j*[j]_f)*b - e_s^j*[j]_f + e_f^j*[j]_s + 2*e_s^j*[j]_s}{2*e_s^j*[j]_s} > \left(\frac{1}{a}\right) \quad \text{(S6.12)}$$

Evaluating the numerator on the left-hand side of this equation:

$$\begin{aligned}([j]_s * [j]_f + e_s^j * [j]_f) * b - e_s^j * [j]_f + e_f^j * [j]_s + 2 * e_s^j * [j]_s \\ = b * [j]_s * [j]_f + b * e_s^j * [j]_f - e_s^j * [j]_f + e_f^j * [j]_s + 2 * e_s^j * [j]_s \\ = (b * [j]_s + b * e_s^j - e_s^j) * [j]_f + e_f^j * [j]_s + 2 * e_s^j * [j]_s\end{aligned}$$

Since $(b * [j]_s + b * e_s^j - e_s^j) > 0$, the numerator should be > 0. The denominator should also be > 0 (as uncertainty cannot be negative). Therefore, a must also be > 0. We can therefore rewrite (S6.12) as:

$$a > \frac{2*e_s^j*[j]_s}{([j]_s*[j]_f + e_s^j*[j]_f)*b - e_s^j*[j]_f + e_f^j*[j]_s + 2*e_s^j*[j]_s} \quad \text{(6a)}$$

1.3 Full derivation of a metric, Φ, for elemental tracer resolvability

To compare between the efficacies of different elemental tracers in a mass-balance framework, we can define a metric, Φ, which demonstrates whether a signal from ERW is sufficient to overcome analytical uncertainty. We define Φ as:

$$\varphi = \frac{|\Delta[i]_{m-s}|}{e^i_{m+s}} \quad (7)$$

We can rewrite (1) for $[i]$, as for $[j]$:

$$e^i_m = e^i_s + (e^i_f - e^i_s) * \frac{[i]_m - [i]_s}{[i]_f - [i]_s} \quad (1i)$$

For $[i]$, as for $[j]$:

$$[i]_m = a * [i]_f + (1-a) * [i]_s \quad (S7)$$

Therefore, substituting (S7) into (7):

$$\varphi = \frac{|a * [i]_f + (1-a) * [i]_s - [i]_s|}{e^i_{m+s}} \quad (S8)$$

Then, substituting (1i) into (S8):

$$\varphi = \frac{|a * [i]_f + (1-a) * [i]_s - [i]_s|}{2e^i_s + (e^i_f - e^i_s) * \frac{[i]_m - [i]_s}{[i]_f - [i]_s}} \quad (S9)$$

Then, substituting (S7) into (S9):

$$\varphi = \frac{|a * [i]_f + (1-a) * [i]_s - [i]_s|}{2e^i_s + (e^i_f - e^i_s) * \frac{a * [i]_f + (1-a) * [i]_s - [i]_s}{[i]_f - [i]_s}} \quad (S10)$$

Simplifying:

$$\varphi = \frac{|a * [i]_f + (1-a) * [i]_s - [i]_s|}{2e^i_s + (e^i_f - e^i_s) * a} \quad (8)$$

In the case where we consider a ratio of immobile trace elements, e.g. $\frac{[i]^\alpha_f}{[i]^\beta_f}$ and $\frac{[i]^\alpha_s}{[i]^\beta_s}$ where α and β are different elements (e.g., Ti and Th), we can rewrite (S7) as follows:

$$\varphi = \frac{\left|\Delta \frac{[i]^\alpha_{m-s}}{[i]^\beta_{m-s}}\right|}{e^{i\left(\frac{\alpha}{\beta}\right)}_{m+s}} \quad (S11)$$

We can rewrite (S7) as follows:

$$\frac{[i]^\alpha_m}{[i]^\beta_m} = \frac{a * [i]^\alpha_f + (1-a) * [i]^\alpha_s}{a * [i]^\beta_f + (1-a) * [i]^\beta_s} \quad (S12)$$

We can rewrite (1i) with error propagation as follows:

$$e_m^{i(\frac{\alpha}{\beta})} = \frac{[i]_m^{\alpha}}{[i]_m^{\beta}} * \sqrt{\left(\frac{e_s^{i\alpha} + (e_f^{i\alpha} - e_s^{i\alpha}) * \frac{[i]_m^{\alpha} - [i]_s^{\alpha}}{[i]_f^{\alpha} - [i]_s^{\alpha}}}{[i]_m^{\alpha}}\right)^2 + \left(\frac{e_s^{i\beta} + (e_f^{i\beta} - e_s^{i\beta}) * \frac{[i]_m^{\beta} - [i]_s^{\beta}}{[i]_f^{\beta} - [i]_s^{\beta}}}{[i]_m^{\beta}}\right)^2} \quad \text{(S13)}$$

Then, substituting from (S12) into (S13):

$$e_m^{i(\frac{\alpha}{\beta})} = \frac{a*[i]_f^{\alpha} + (1-a)*[i]_s^{\alpha}}{a*[i]_f^{\beta} + (1-a)*[i]_s^{\beta}} * \sqrt{\left(\frac{e_s^{i\alpha} + (e_f^{i\alpha} - e_s^{i\alpha}) * \frac{a*[i]_f^{\alpha} + (1-a)*[i]_s^{\alpha} - [i]_s^{\alpha}}{[i]_f^{\alpha} - [i]_s^{\alpha}}}{a*[i]_f^{\alpha} + (1-a)*[i]_s^{\alpha}}\right)^2 + \left(\frac{e_s^{i\beta} + (e_f^{i\beta} - e_s^{i\beta}) * \frac{a*[i]_f^{\beta} + (1-a)*[i]_s^{\beta} - [i]_s^{\beta}}{[i]_f^{\beta} - [i]_s^{\beta}}}{a*[i]_f^{\beta} + (1-a)*[i]_s^{\beta}}\right)^2} \quad \text{(S14)}$$

Propagating error for soil:

$$e_s^{i(\frac{\alpha}{\beta})} = \frac{[i]_s^{\alpha}}{[i]_s^{\beta}} * \sqrt{\left(\frac{e_s^{i\alpha}}{[i]_s^{\alpha}}\right)^2 + \left(\frac{e_s^{i\beta}}{[i]_s^{\beta}}\right)^2} \quad \text{(S15)}$$

Substituting (S12) into (S11):

$$\varphi = \frac{\left|\frac{a*[i]_f^{\alpha} + (1-a)*[i]_s^{\alpha}}{a*[i]_f^{\beta} + (1-a)*[i]_s^{\beta}} - \frac{[i]_s^{\alpha}}{[i]_s^{\beta}}\right|}{e_{m+s}^{i(\frac{\alpha}{\beta})}} \quad \text{(S16)}$$

Then, substituting (S14) and (S15) into (S16):

$$\varphi = \frac{\left|\frac{a*[i]_f^{\alpha} + (1-a)*[i]_s^{\alpha}}{a*[i]_f^{\beta} + (1-a)*[i]_s^{\beta}} - \frac{[i]_s^{\alpha}}{[i]_s^{\beta}}\right|}{\frac{a*[i]_f^{\alpha} + (1-a)*[i]_s^{\alpha}}{a*[i]_f^{\beta} + (1-a)*[i]_s^{\beta}} * \sqrt{\left(\frac{e_s^{i\alpha} + (e_f^{i\alpha} - e_s^{i\alpha}) * \frac{a*[i]_f^{\alpha} + (1-a)*[i]_s^{\alpha} - [i]_s^{\alpha}}{[i]_f^{\alpha} - [i]_s^{\alpha}}}{a*[i]_f^{\alpha} + (1-a)*[i]_s^{\alpha}}\right)^2 + \left(\frac{e_s^{i\beta} + (e_f^{i\beta} - e_s^{i\beta}) * \frac{a*[i]_f^{\beta} + (1-a)*[i]_s^{\beta} - [i]_s^{\beta}}{[i]_f^{\beta} - [i]_s^{\beta}}}{a*[i]_f^{\beta} + (1-a)*[i]_s^{\beta}}\right)^2} + \frac{[i]_s^{\alpha}}{[i]_s^{\beta}} * \sqrt{\left(\frac{e_s^{i\alpha}}{[i]_s^{\alpha}}\right)^2 + \left(\frac{e_s^{i\beta}}{[i]_s^{\beta}}\right)^2}} \quad \text{(S17)}$$

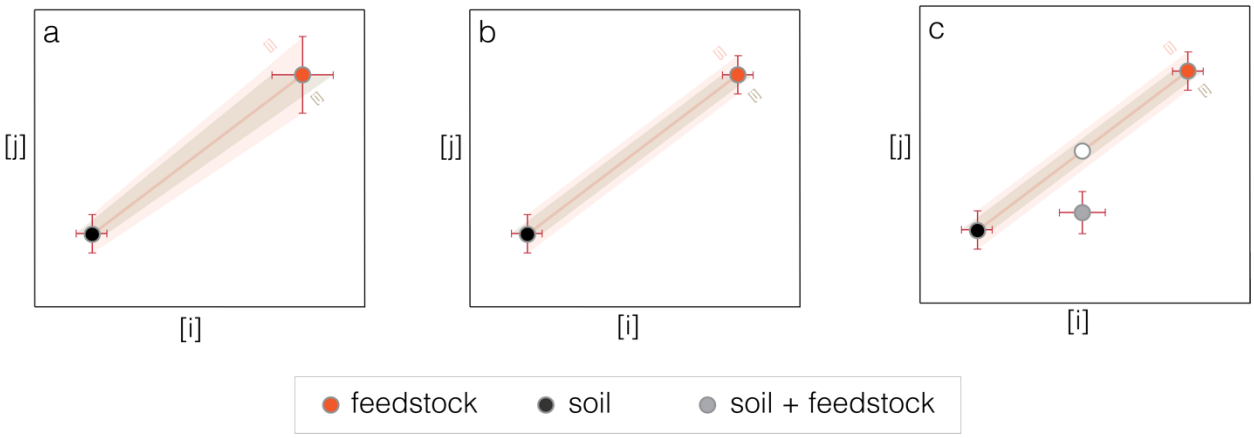

Figure S1: Theoretical two-endmember mixing plots showing an immobile element, *i*, plotted against a mobile element, *j*. (a) The same uncertainty (in %) for the feedstock endmember (c_f, red circle) is 2x greater in absolute terms than for the soil endmember (c_s, black circle) if the concentration of the feedstock is 2x that of the soil. In this case, the greater the concentration of feedstock in a homogeneous mixture that falls on the mixing line, the larger the uncertainty envelope for [*i*] and [*j*]. (b) As in (a), but here absolute uncertainty for the feedstock endmember is the same as for the soil endmember, due to theoretical replicate analyses. Here, uncertainty as a % of concentration for feedstock is 1/2x that of soil. (c) Here the mixture after weathering (grey circle) has absolute uncertainty in [*i*] that is 1.5x the soil endmember, but absolute uncertainty in [*j*] that is only 1.1x the soil endmember, given its lower absolute concentration [*j*] than that of a mixture plotting onto the mixing line pre-weathering (white circle).

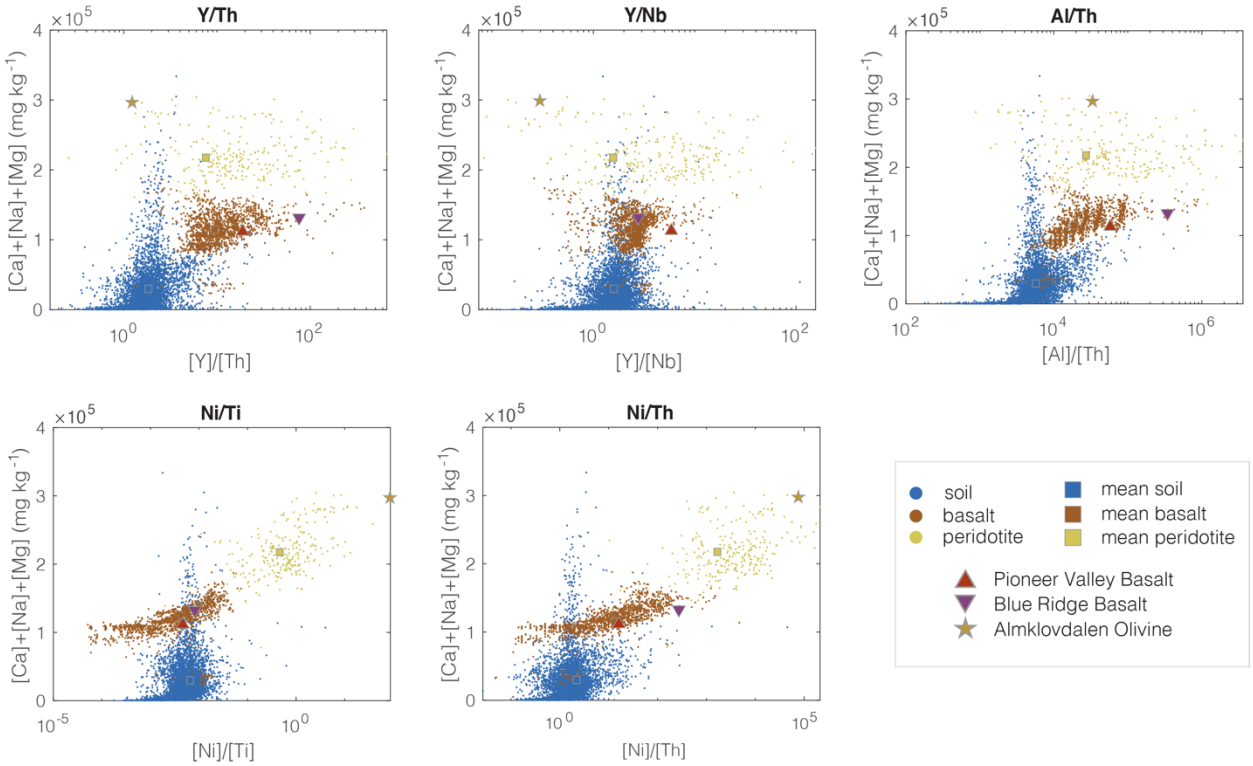

Figure S2: Cross-plots of sum mobile cation concentrations vs. the concentrations of additional (compared to Figure 1) different (partially) immobile elements that may be used as tracers in mass-balance MRV approaches for ERW. Soil data are from the USGS 'Geochemical and mineralogical data for soils of the conterminous United States' database (n = 4,841) (Smith et al., 2013). Basalt and peridotite (including Almklovdalen Olivine) data are extracted from the GEOROC database (Lehnert et al., 2000); see main text for more details on selection criteria and Datasheet 1 for feedstock compositions.

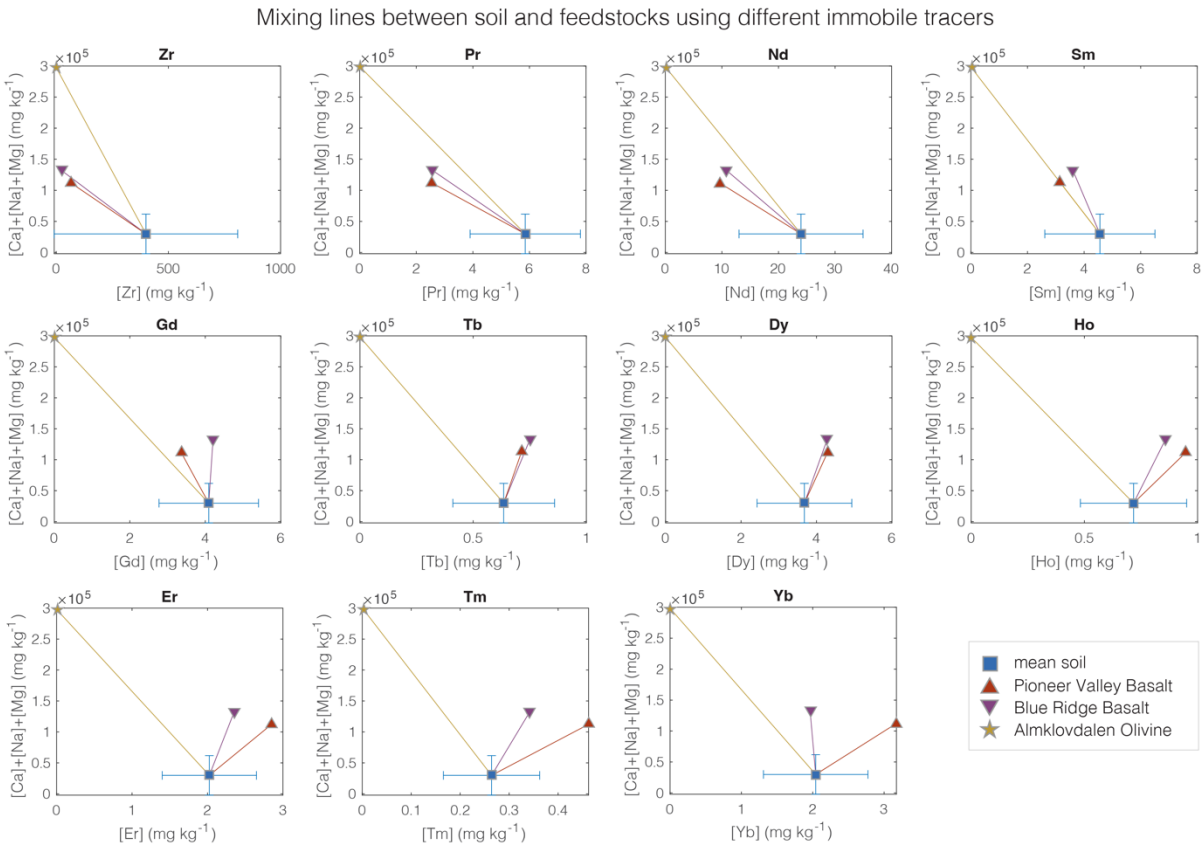

Figure S3: Mixing lines between soil and feedstock endmembers in mobile cation vs. immobile element space for REE elements as well as Zr not contained in the USGS database. Shown are specific feedstock compositions and average soil concentrations. The panels demonstrate the lever between soil and feedstock compositions; the larger the difference in both cation and *i* space; the easier it is to quantify feedstock addition. These REE (and Zr) data are not contained in the USGS database; data shown are global average (± 1SD) soil concentrations based on data from 32 countries (Laul et al., 1979; Markert, 1987; Markert & De Li, 1991; Diatloff et al., 1996; Öhlander et al., 1996; Yoshida et al., 1998; Smith et al., 2000; Tyler & Olsson, 2002; Lijun W. et al., 2004; Takeda et al., 2004; Salminen et al., 2005; Caspari et al., 2006; Uchida et al., 2007; Miao et al., 2008; Zhang et al., 2008; El-Ramady, 2010; Loell et al., 2011; Smidt et al., 2011; Cheng et al., 2012; Marques et al., 2012; Oliveira et al., 2012; Li et al., 2013; Sadeghi et al., 2013; Moreira, 2014) compiled in (Ramos et al., 2016). Zirconium concentration is based on compiled data (Bowen, 1979; Pais & Jones Jr, 1997; Kabata-Pendias & Pendias, 2003; Fodor et al., 2005) reported in (Shahid et al., 2013). Soil cation data are mean soil concentrations based on the USGS 'Geochemical and mineralogical data for soils of the conterminous United States' database (n = 4,841; shown is mean ± 1SD) (Smith et al., 2013). Almklovdalen Olivine data are extracted from the GEOROC database (Lehnert et al., 2000). Composition of Pioneer Valley Basalt and Blue Ridge Basalt feedstocks can be found in Datasheet 1.

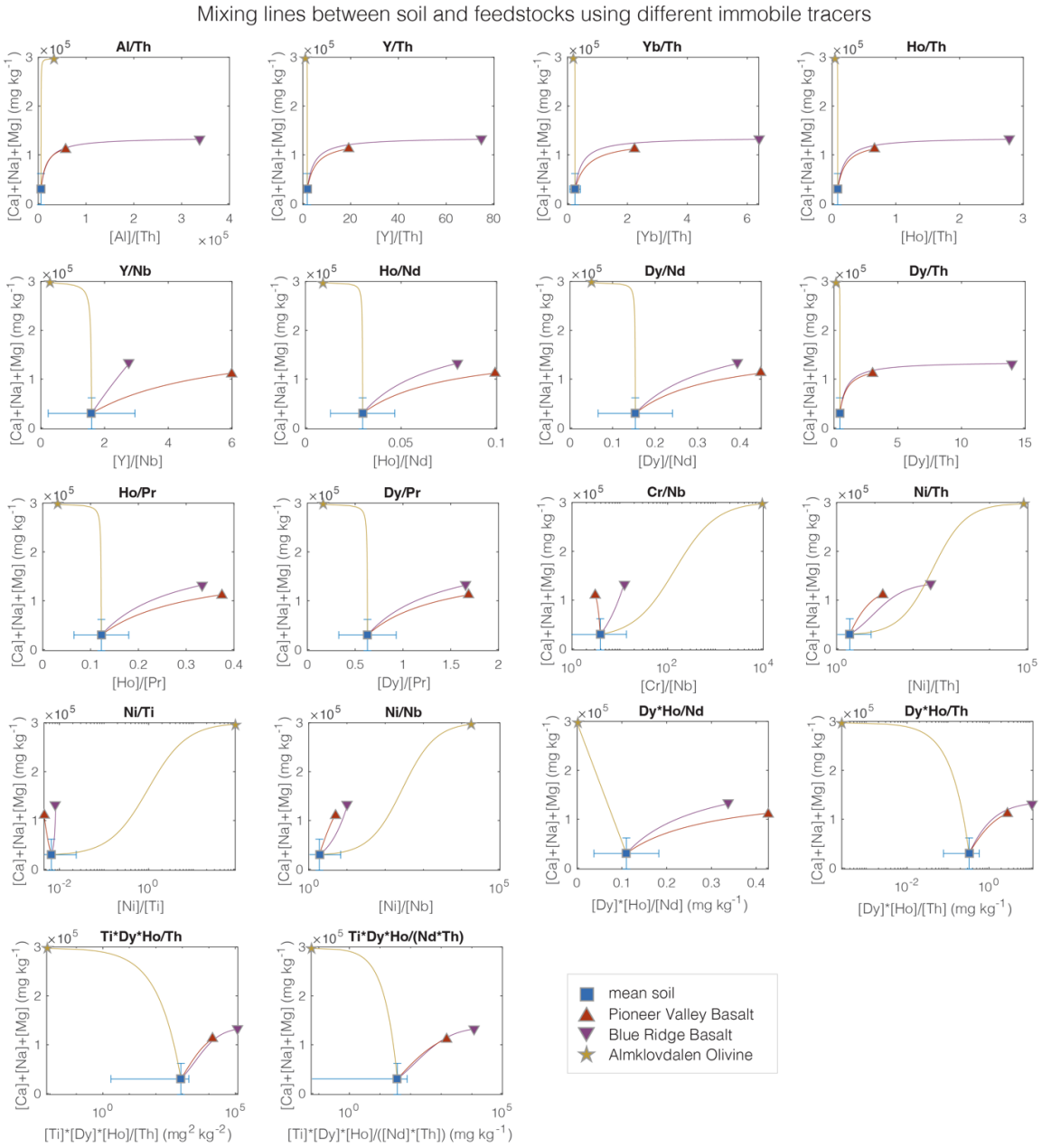

Figure S4: Same data as in Figure S3 (and Figure 2 For Al, Th, Y, Nb, Ni, Cr, Ti), but using ratios of immobile elements that may be useful at detecting EW signals. Shown are specific feedstock compositions and average soil concentrations of 32 countries (Ramos et al., 2016); see main text for all references for individual countries. Mixing lines for immobile element ratios form curves (note that Cr/Th and Cr/Ti have a different shape due to the logarithmic x-axis), as would be expected for soil-feedstock mixing with different concentrations of both immobile elements. The shape of the mixing curve has important implications for resolvability; the more vertical its trajectory from the mean soil composition, the more difficult feedstock addition resolvability based on φ because the immobile element ratio changes little in $\frac{i^{\alpha}}{i^{\beta}}$ space at low mixing ratios. See also Figure S3 for additional *i* not contained in the USGS database.

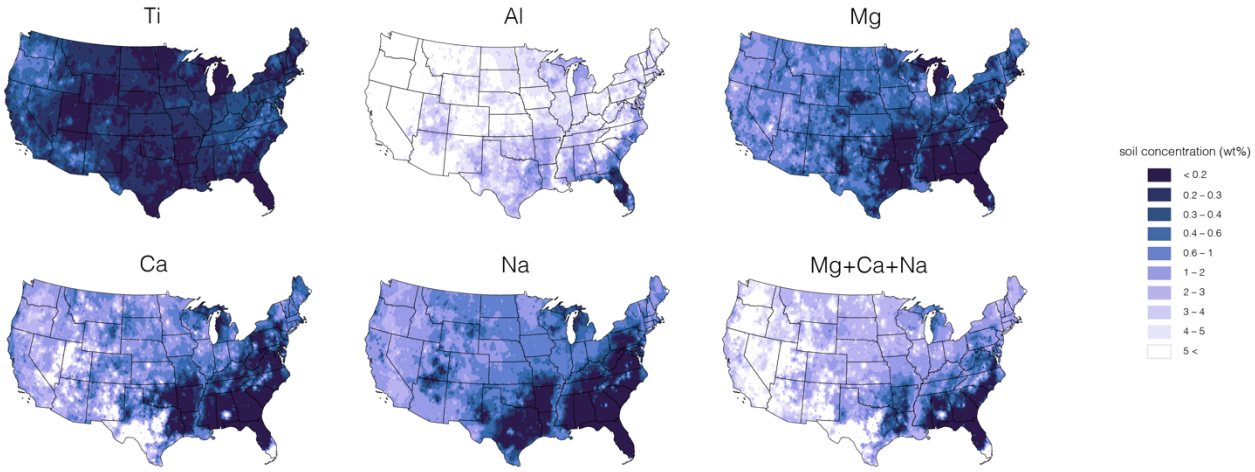

Figure S5: Maps of concentrations of Ti, Al, Mg, Ca, Na, as well as sum of Mg, Ca, and Na in topsoils (0-5cm) throughout the US. Data is based on the semi-gridded USGS 'Geochemical and mineralogical data for soils of the conterminous United States' dataset (Smith et al., 2013).

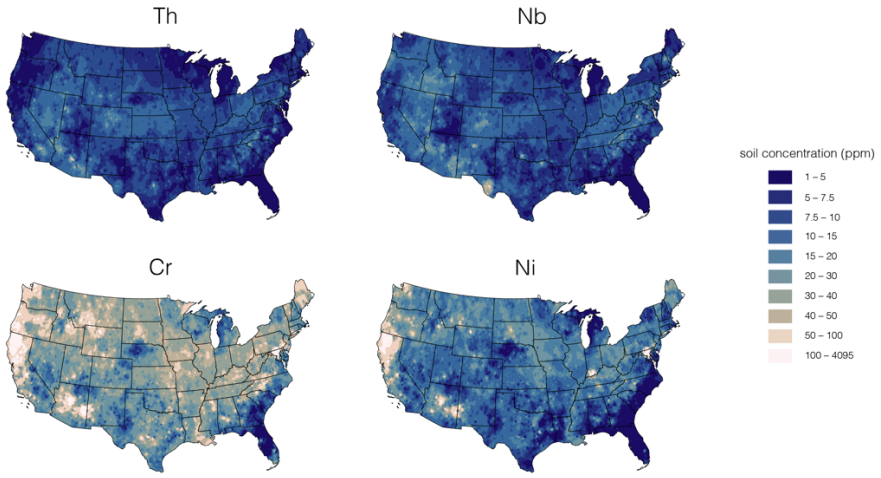

Figure S6: Maps of Th, Nb, Cr, and Ni concentrations in topsoils (0-5cm) throughout the US. Data is based on the semi-gridded USGS 'Geochemical and mineralogical data for soils of the conterminous United States' dataset (Smith et al., 2013).

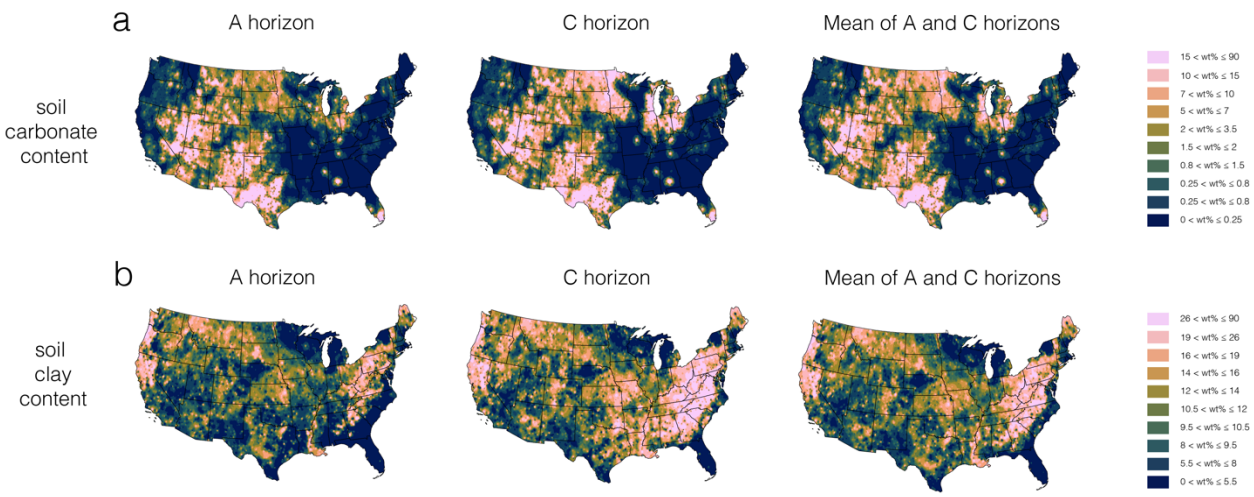

Figure S7: Distribution of soil carbonate (dolomite + carbonate) and clay (total clays; sum of kaolinite, and 10 and 14 Å clays; see Smith et al. (2013) for discussion on uncertainties) content in in different soil horizons throughout the conterminous US. Data are sourced from the 'Geochemical and mineralogical data for soils of the conterminous United States' database (Smith et al., 2013).

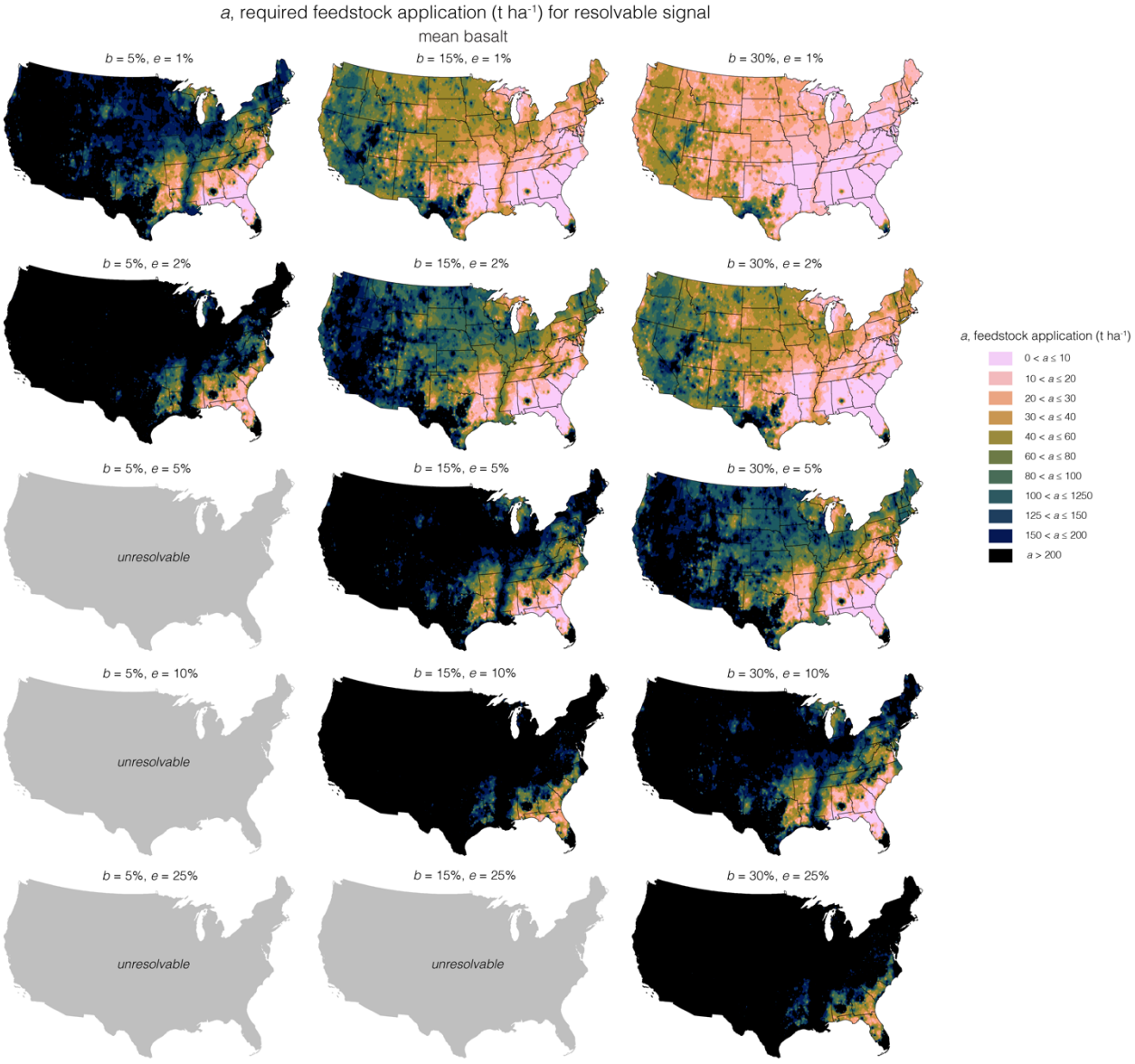

Figure S8: Requisite mean basalt feedstock application for enhanced weathering to be detectable through mobile cation loss based on assumed values of feedstock dissolution (b = 5, 15, and 30%) and (aggregated analytical and sampling) uncertainty (e = 1, 2, 5, 10, and 25%). For low dissolution rates and high uncertainties, feedstock dissolution cannot be resolved (panel with b = 5%, e = 5%; see main text for more detail).

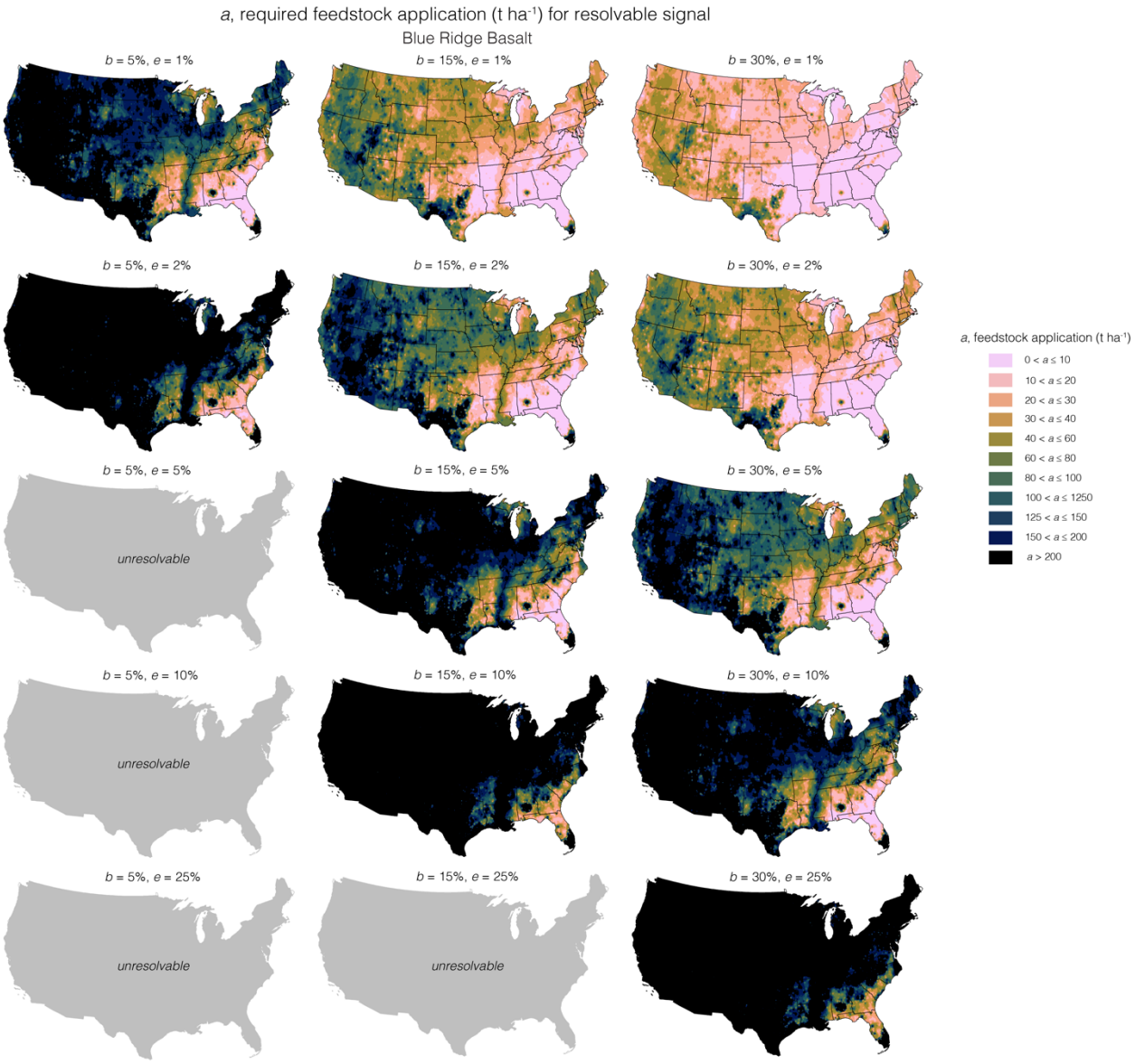

Figure S9: Requisite Blue Ridge Basalt feedstock application for enhanced weathering to be detectable through mobile cation loss based on assumed values of feedstock dissolution (b = 5, 15, and 30%) and (aggregated analytical and sampling) uncertainty (e = 1, 2, 5, 10**,** and 25%). For low dissolution rates and high uncertainties, feedstock dissolution cannot be resolved (panel with b = 5%, e = 5%; see main text for more detail).

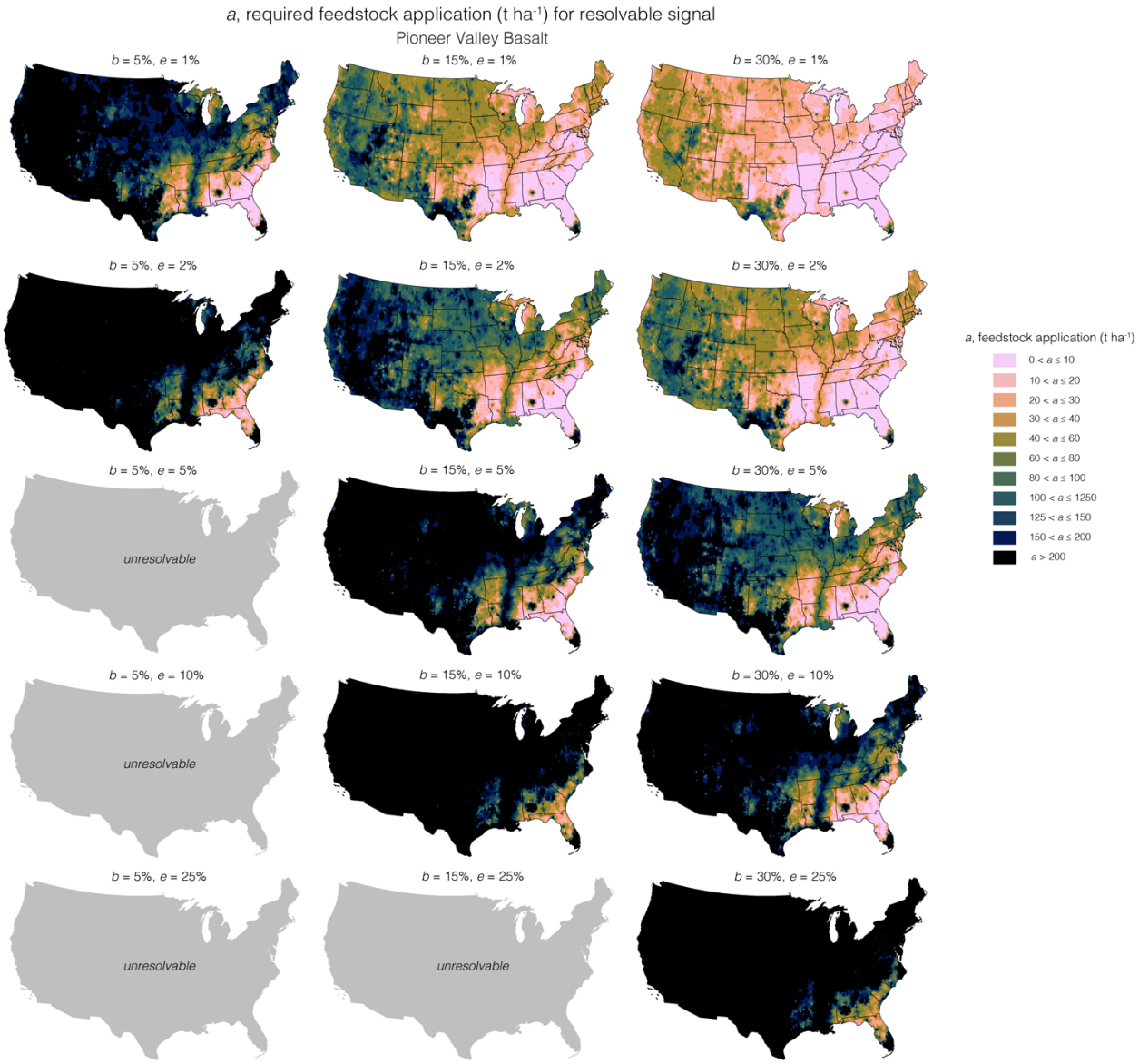

Figure S10: Requisite Pioneer Valley Basalt feedstock application for enhanced weathering to be detectable through mobile cation loss based on assumed values of feedstock dissolution (b = 5, 15, and 30%) and (aggregated analytical and sampling) uncertainty (e = 1, 2, 5, 10**,** and 25%). For low dissolution rates and high uncertainties, feedstock dissolution cannot be resolved (panel with b = 5%, e = 5%; see main text for more detail).

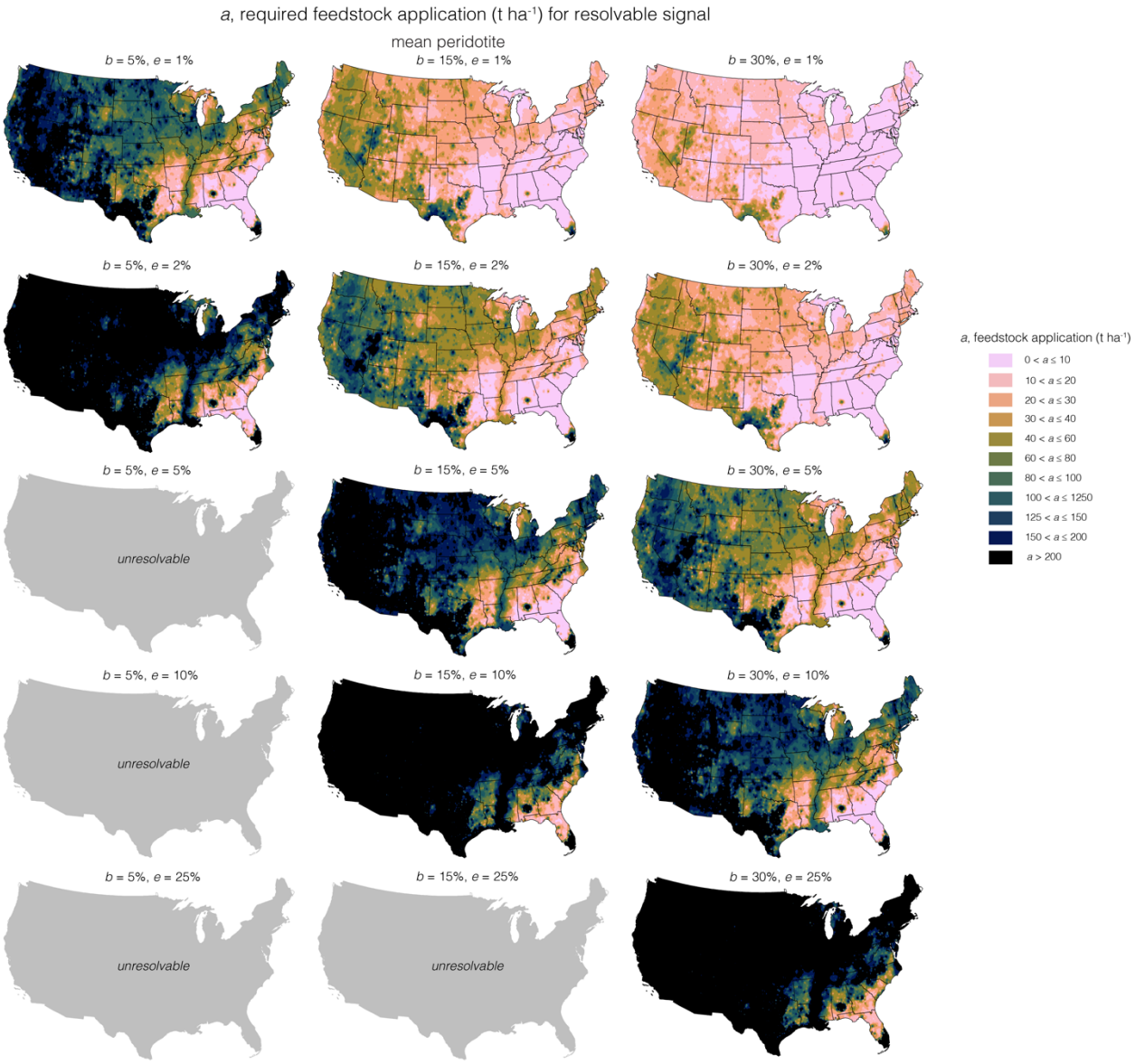

Figure S11: Requisite mean peridotite feedstock application for enhanced weathering to be detectable through mobile cation loss based on assumed values of feedstock dissolution (b = 5, 15, and 30%) and (aggregated analytical and sampling) uncertainty (e = 1, 2, 5, 10**,** and 25%). For low dissolution rates and high uncertainties, feedstock dissolution cannot be resolved (panel with b = 5%, e = 5%; see main text for more detail).

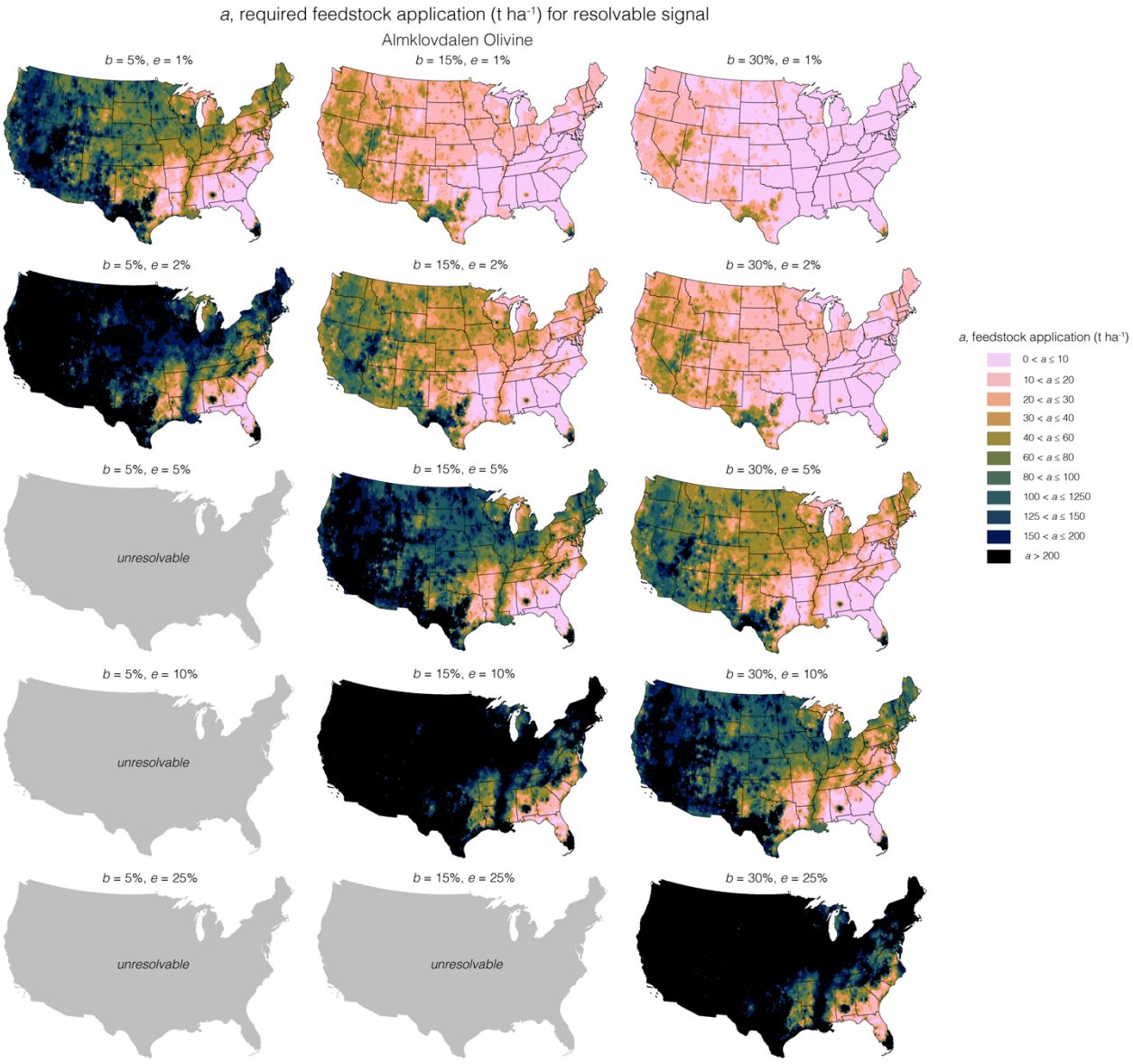

Figure S12: Requisite Almklodalen Olivine feedstock application for enhanced weathering to be detectable through mobile cation loss based on assumed values of feedstock dissolution (b = 5, 15, and 30%) and (aggregated analytical and sampling) uncertainty (e = 1, 2, 5, 10**,** and 25%). For low dissolution rates and high uncertainties, feedstock dissolution cannot be resolved (panel with b = 5%, e = 5%; see main text for more detail).

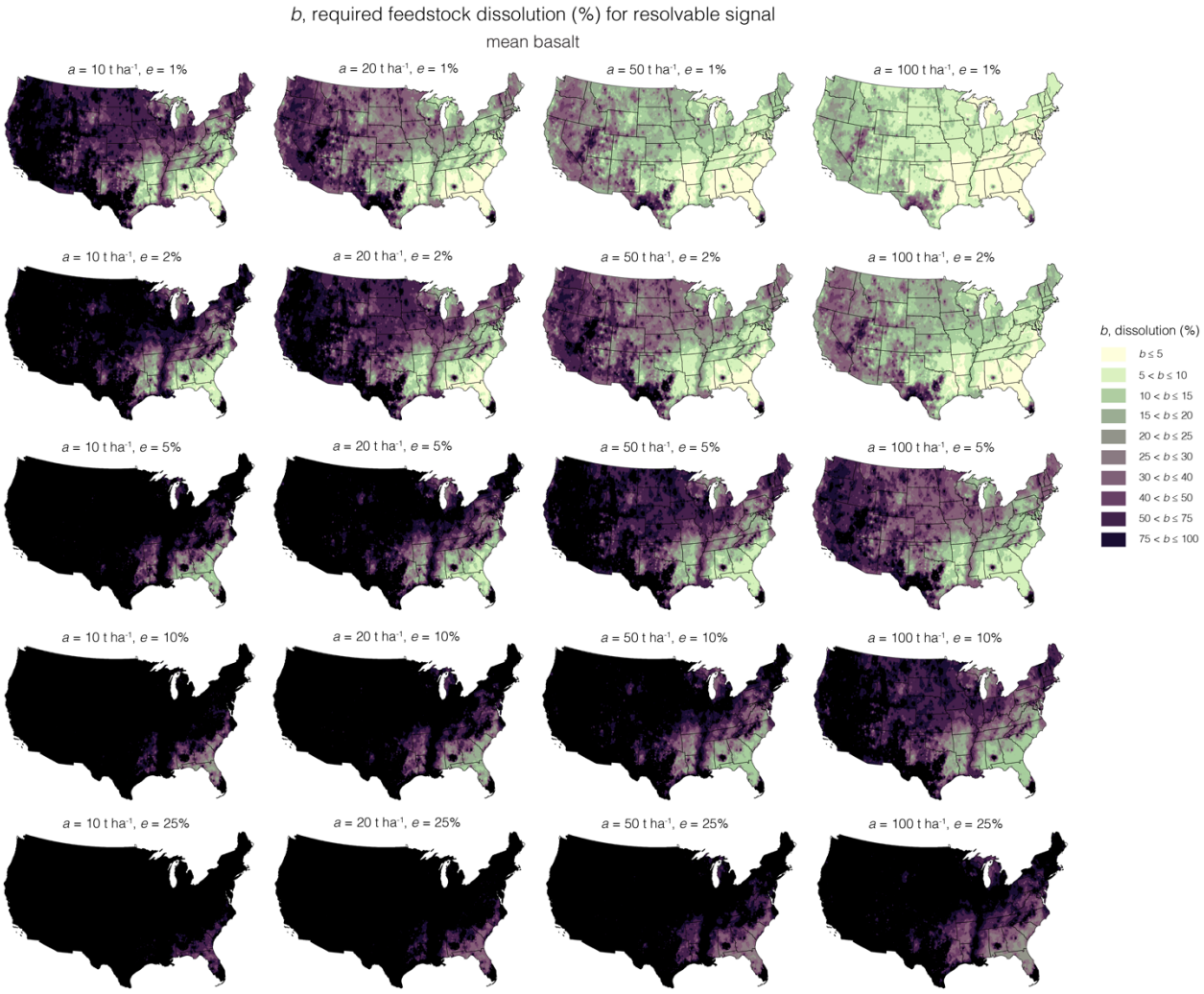

Figure S13: Required mean basalt feedstock dissolution for enhanced weathering to be detectable through mobile cation loss based on assumed values of feedstock addition (a = 10, 20, 50, and 100 t ha^{-1}) and (aggregated analytical and sampling) uncertainty (e = 1, 2, 5, 10, and 25%).

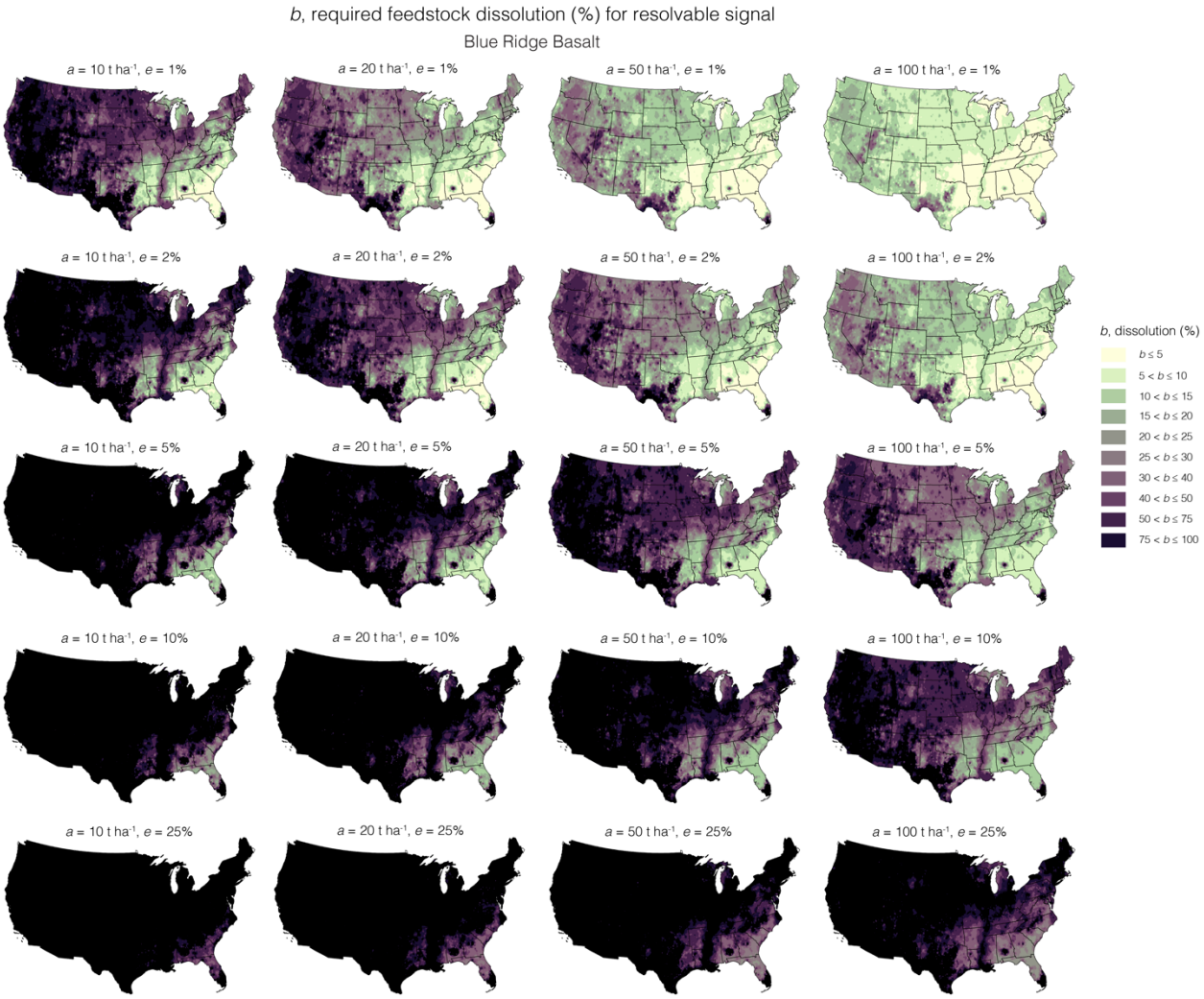

Figure S14: Required Blue Ridge Basalt feedstock dissolution for enhanced weathering to be detectable through mobile cation loss based on assumed values of feedstock addition (a = 10, 20, 50, and 100 t ha^{-1}) and (aggregated analytical and sampling) uncertainty (e = 1, 2, 5, 10, and 25%).

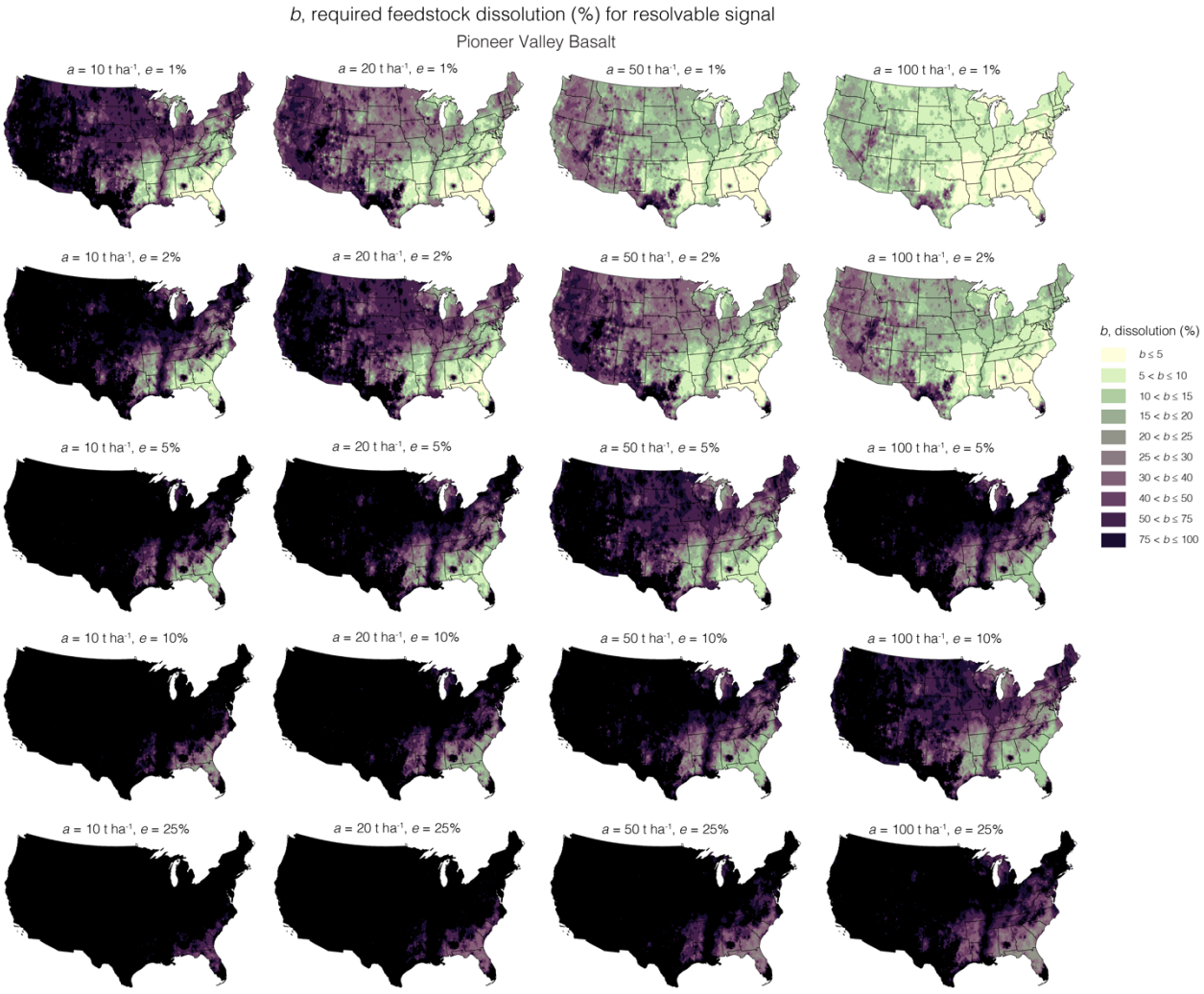

Figure S15: Required Pioneer Valley Basalt feedstock dissolution for enhanced weathering to be detectable through mobile cation loss based on assumed values of feedstock addition *(a* = 10, 20, 50, and 100 t ha^{-1}) and (aggregated analytical and sampling) uncertainty (*e* = 1, 2, 5, 10, and 25%).

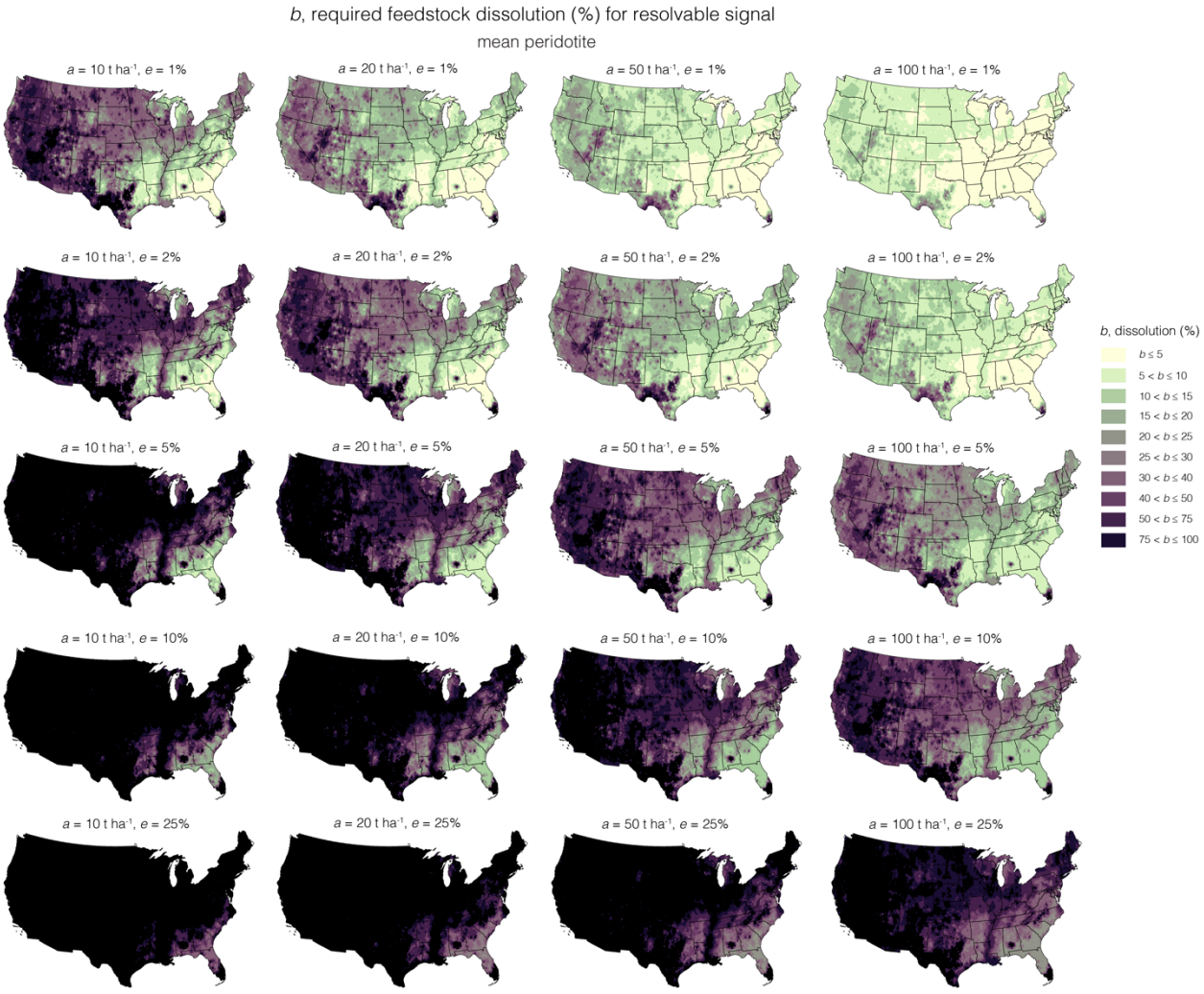

Figure S16: Required mean peridotite feedstock dissolution for enhanced weathering to be detectable through mobile cation loss based on assumed values of feedstock addition (a = 10, 20, 50, and 100 t ha^{-1}) and (aggregated analytical and sampling) uncertainty (e = 1, 2, 5, 10, and 25%).

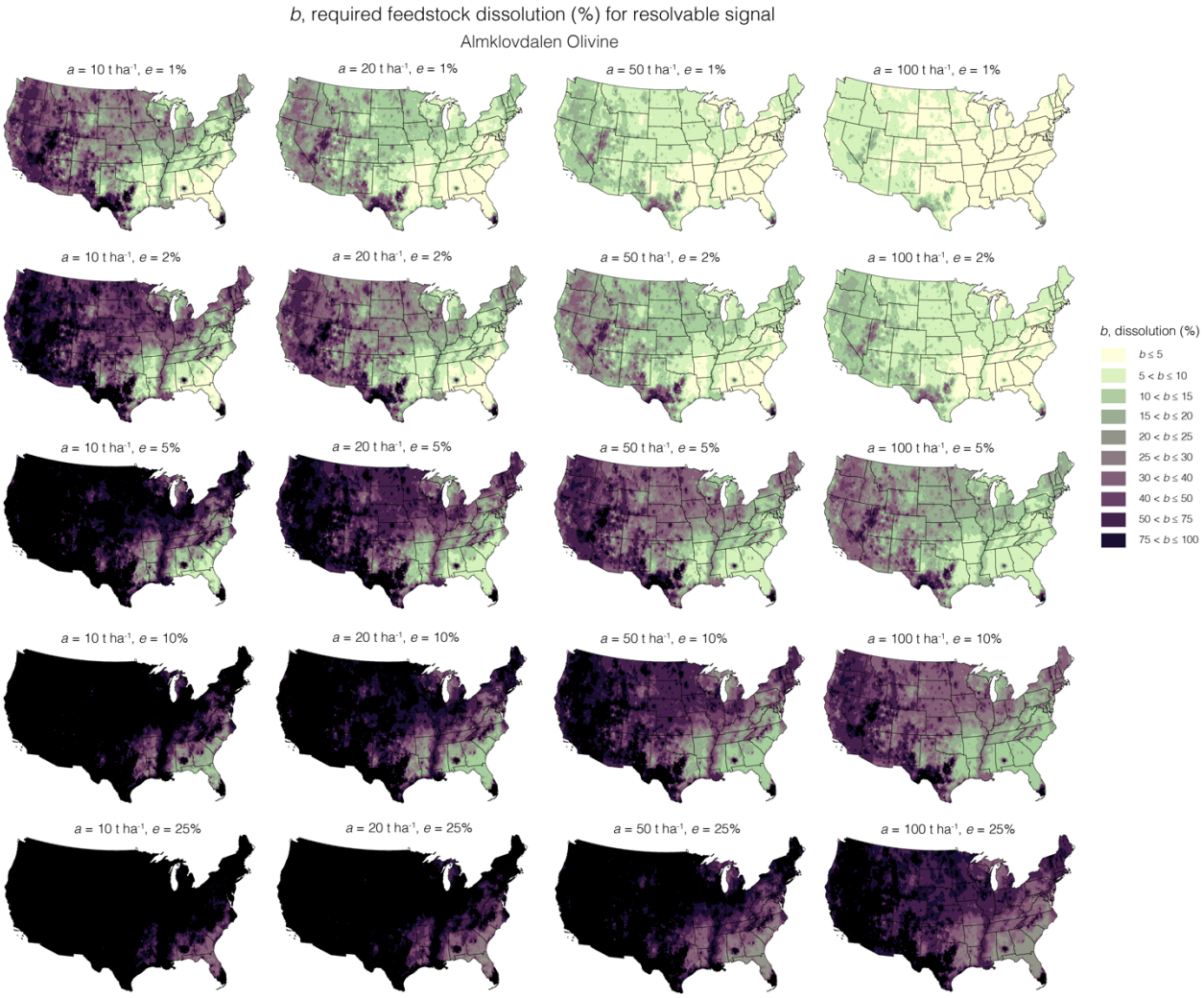

Figure S17: Required Almklovdalen Olivine feedstock dissolution for enhanced weathering to be detectable through mobile cation loss based on assumed values of feedstock addition (a = 10, 20, 50, and 100 t ha^{-1}) and (aggregated analytical and sampling) uncertainty (e = 1, 2, 5, 10, and 25%).

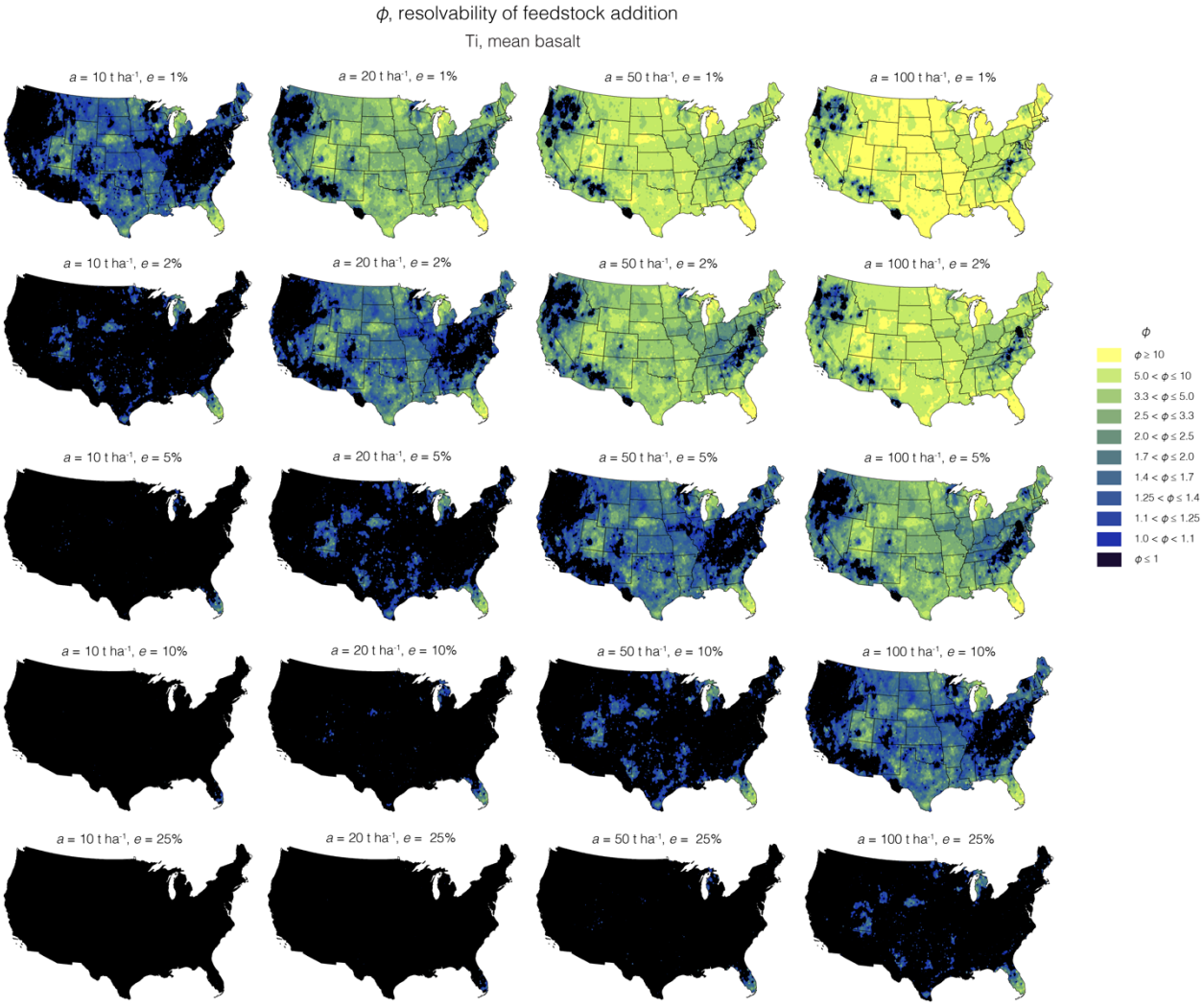

Figure S18: Resolvability of mean basalt feedstock addition (φ) when using Ti as a proxy (*i*) of the addition of mean basalt to US top soils for different assumed values of feedstock addition (*a* = 10, 20, 50, and 100 t ha^{-1}) and (aggregated analytical and sampling) uncertainty (*e* = 1, 2, 5, 10, and 25%). The resolvability increases with higher *a* and lower *e*.

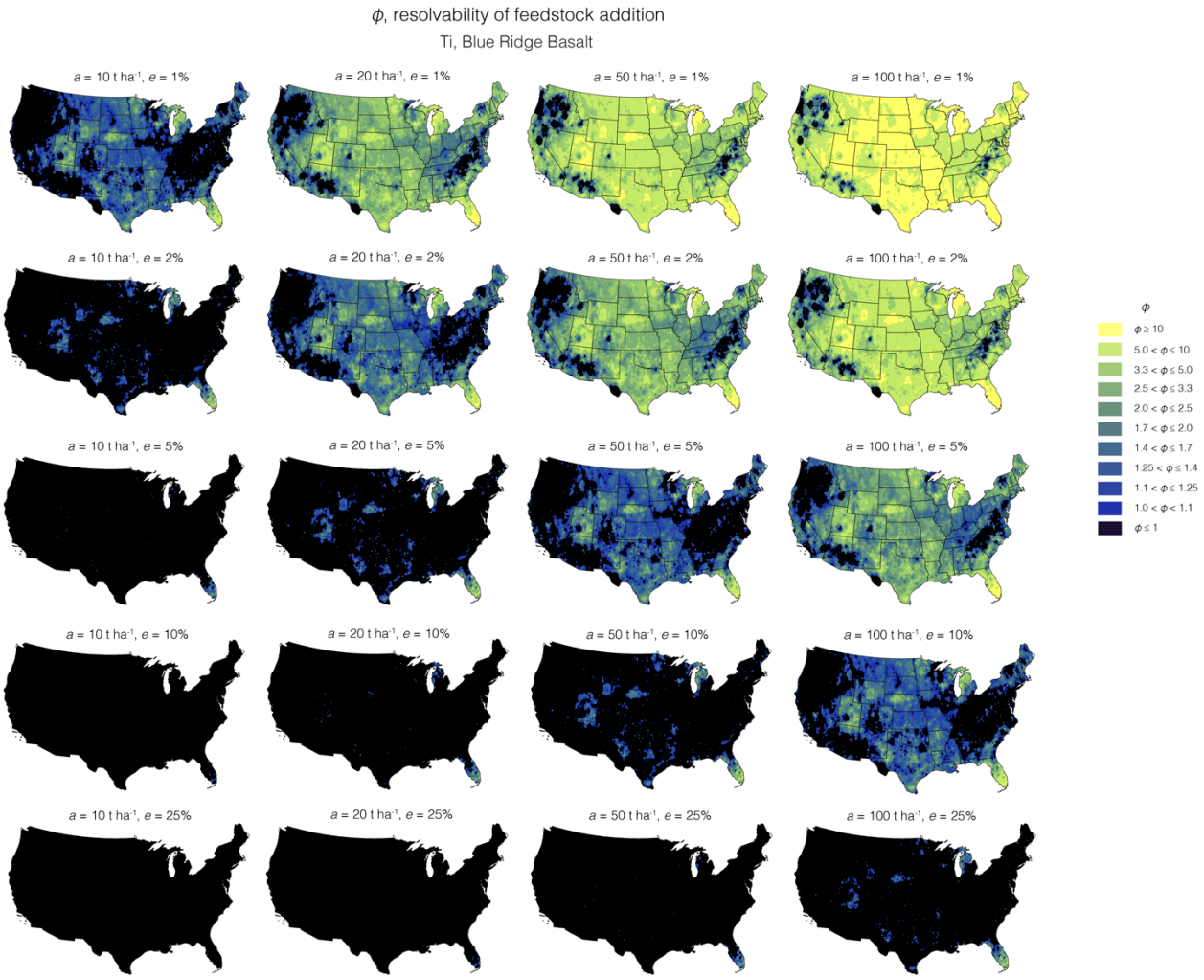

Figure S19: Resolvability of Blue Ridge Basalt feedstock addition (φ) when using Ti as a proxy (*i*) of the addition of mean basalt to US top soils for different assumed values of feedstock addition (a = 10, 20, 50, and 100 t ha^{-1}) and (aggregated analytical and sampling) uncertainty (e = 1, 2, 5, 10, and 25%). The resolvability increases with higher a and lower e**.**

Figure S20: Resolvability of Pioneer Valley Basalt feedstock addition (φ) when using Ti as a proxy (*i*) of the addition of mean basalt to US top soils for different assumed values of feedstock addition (*a* = 10, 20, 50, and 100 t ha^{-1}) and (aggregated analytical and sampling) uncertainty (*e* = 1, 2, 5, 10, and 25%). The resolvability increases with higher *a* and lower *e*.

Figure S21: Resolvability of mean peridotite feedstock addition (φ) when using Ti as a proxy (*i*) of the addition of mean basalt to US top soils for different assumed values of feedstock addition (*a* = 10, 20, 50, and 100 t ha^{-1}) and (aggregated analytical and sampling) uncertainty (*e* = 1, 2, 5, 10, and 25%). The resolvability increases with higher *a* and lower *e*. The apparent resolvability for mean peridotite (and Almklovdalen Olivine) presents an overestimation of resolvability φ when the enrichment of *i* in post-weathering soil+feedstock samples is taken into account – see Figure S36 (and caption) for more detail. In general, the framework presented here only applies for soil-feedstock combinations where *i* is larger in feedstocks than soils. Solid-based mass balance approaches are not feasible for soil-feedstock combinations where *i* is lower in feedstock than soils – at least not accurately (Reershemius & Suhrhoff, 2023; Reershemius & Kelland et al., 2023) Figure S21 demonstrates the importance of taken this into account; if not resolvability φ is overestimated.

Figure S22: Resolvability of Almklovdalen Olivine feedstock addition (φ) when using Ti as a proxy (*i*) of the addition of mean basalt to US top soils for different assumed values of feedstock addition (*a* = 10, 20, 50, and 100 t ha^{-1}) and (aggregated analytical and sampling) uncertainty (*e* = 1, 2, 5, 10, and 25%). The apparent resolvability for Almklovdalen Olivine (and in fact mean peridotite) presents an overestimation of resolvability φ when the enrichment of *i* in post-weathering soil+feedstock samples is taken into account – see Figure S36 (and caption) for more detail. In general, the framework presented here only applies for soil-feedstock combinations where *i* is larger in feedstocks than soils. Solid-based mass balance approaches are not feasible for soil-feedstock combinations where *i* is lower in feedstock than soils – at least not accurately (Reershemius & Suhrhoff, 2023; Reershemius & Kelland et al., 2023) Figure S22 demonstrates the importance of taking this into account; if not resolvability φ is overestimated.

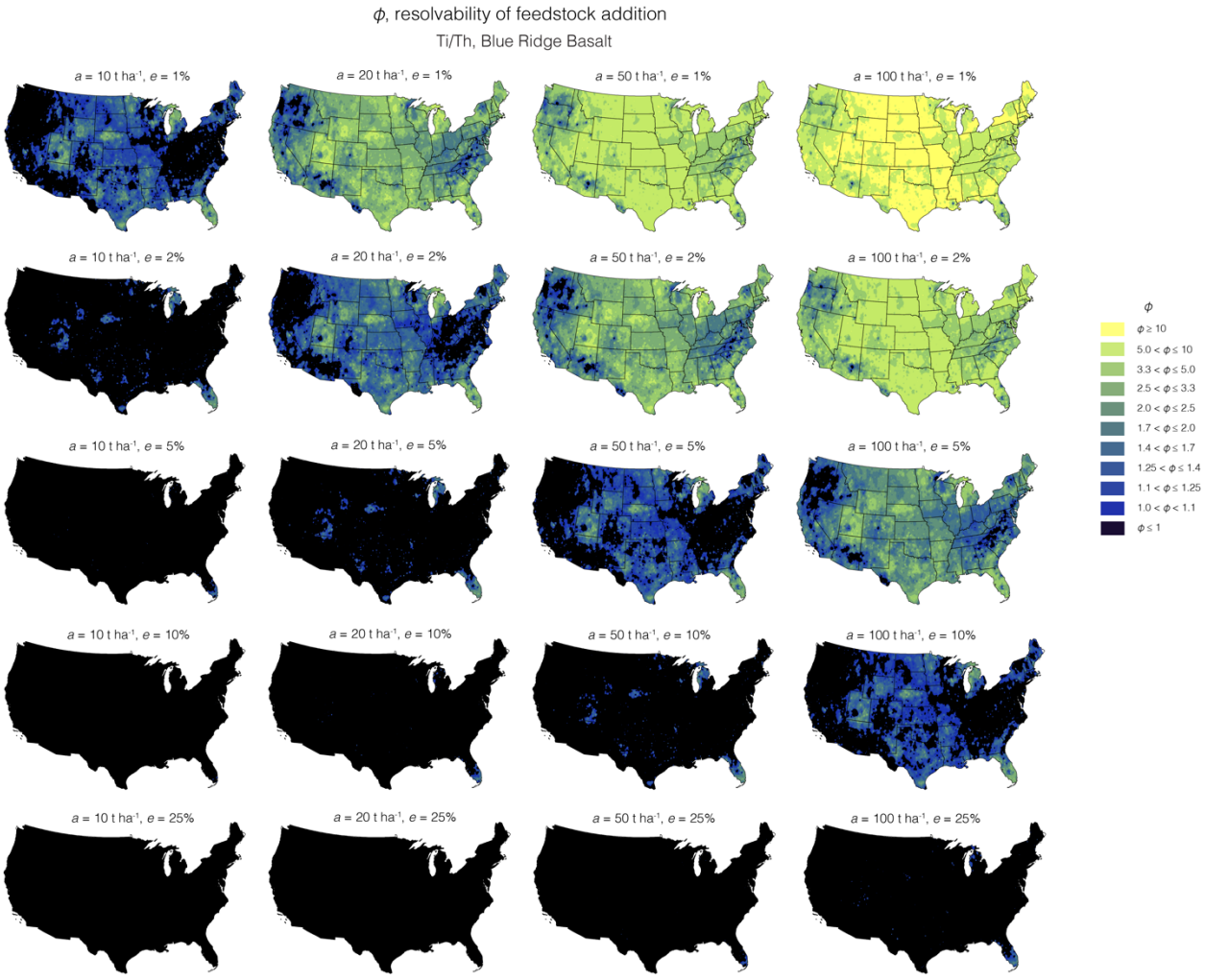

Figure S23: Resolvability of Blue Ridge Basalt feedstock addition (φ) when using Ti/Th as a proxy for the addition of mean basalt to US top soils for different assumed values of feedstock addition (a = 10, 20, 50, and 100 t ha^{-1}) and (aggregated analytical and sampling) uncertainty (e = 1, 2, 5, 10, and 25%). The resolvability increases with higher a and lower e**.**

Figure S24: Resolvability of Pioneer Valley Basalt feedstock addition (φ) when using Ti/Th as a proxy for the addition of mean basalt to US top soils for different assumed values of feedstock addition (a = 10, 20, 50, and 100 t ha-1) and (aggregated analytical and sampling) uncertainty (e = 1, 2, 5, 10, and 25%). The resolvability increases with higher a and lower e**.**

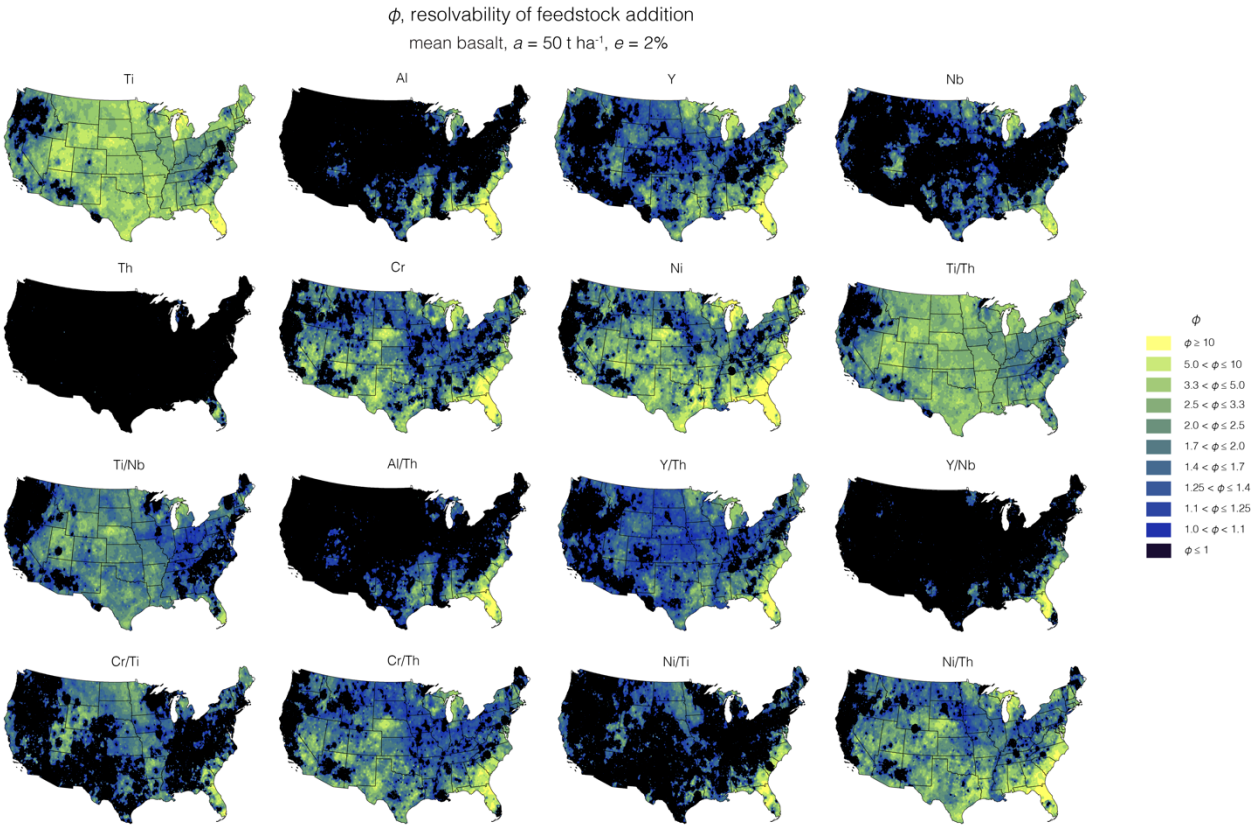

Figure S25: Comparison of the resolvability of feedstock addition (φ) for mean basalt based on different proxies of feedstock addition (i), assuming a = 50 t ha^{-1} and e = 2%.

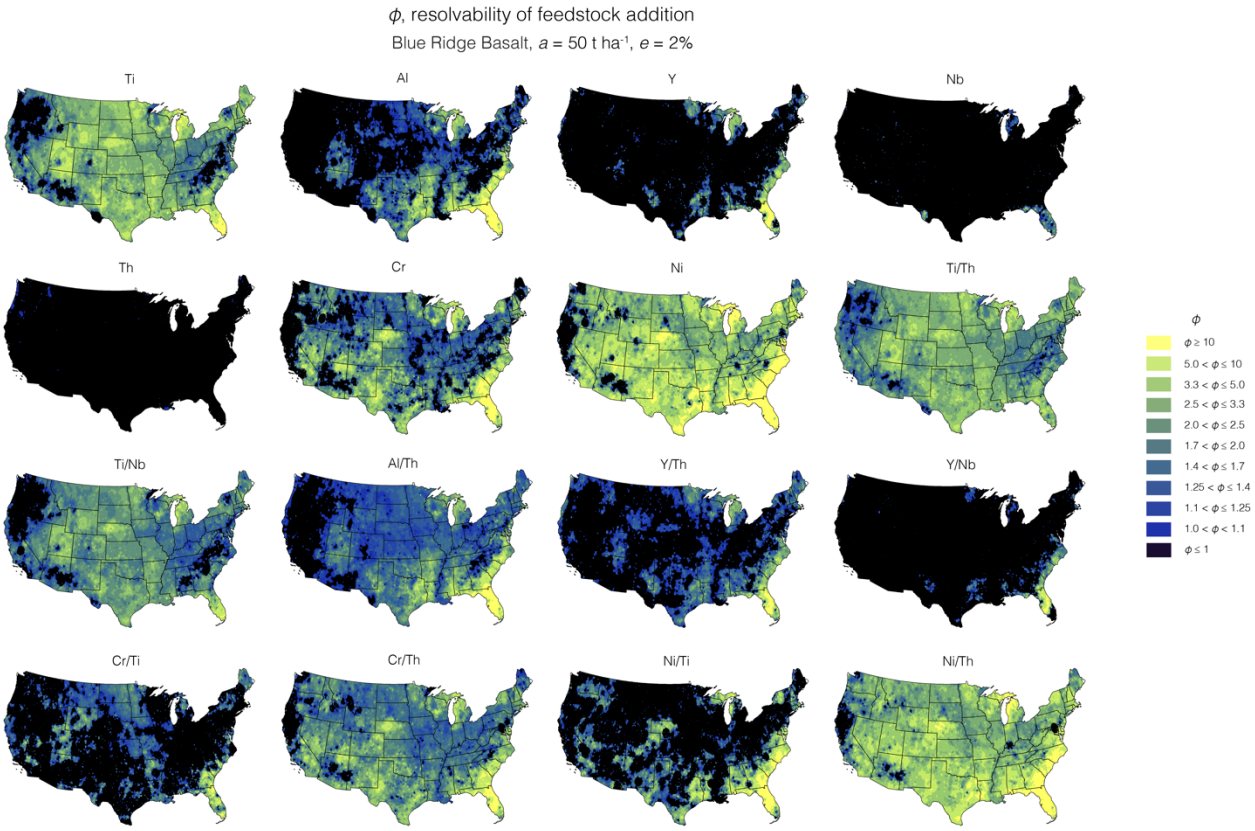

Figure S26: Comparison of the resolvability of feedstock addition (φ) for Blue Ridge Basalt based on different proxies of feedstock addition (i), assuming a = 50 t ha^{-1} and e = 2%.

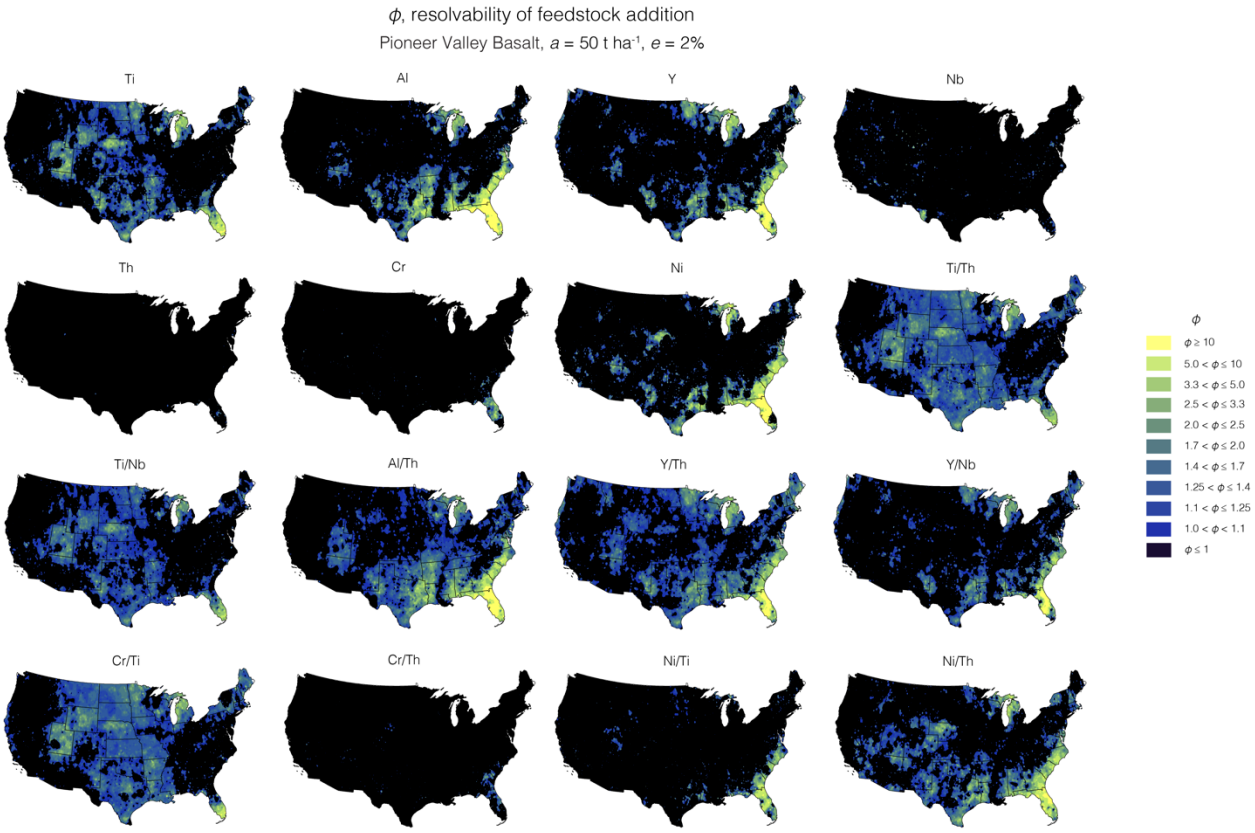

Figure S27: Comparison of the resolvability of feedstock addition (φ) for Pioneer Valley Basalt based on different proxies of feedstock addition (i), assuming a = 50 t ha^{-1} and e = 2%.

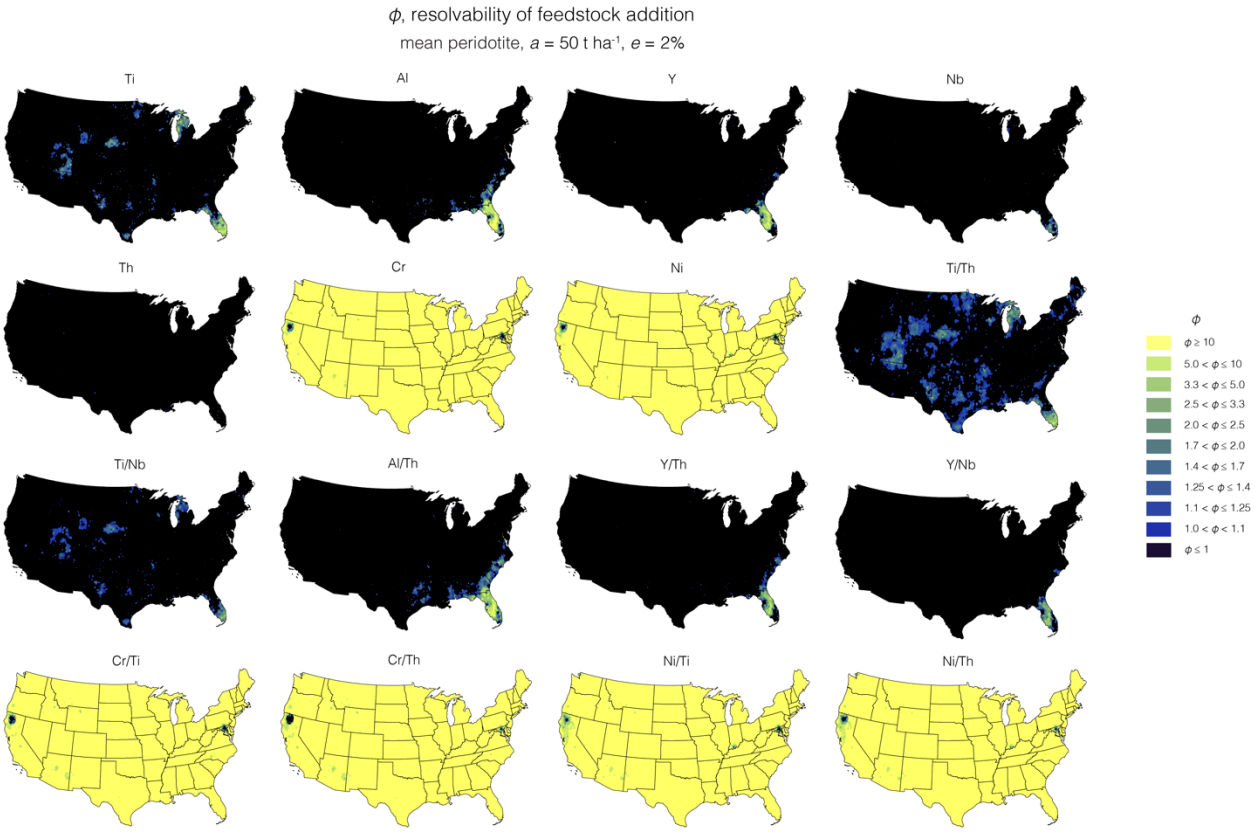

Figure S28: Comparison of the resolvability of feedstock addition (φ) for mean peridotite based on different proxies of feedstock addition (*i*), assuming a = 50 t ha^{-1} and e = 2%.

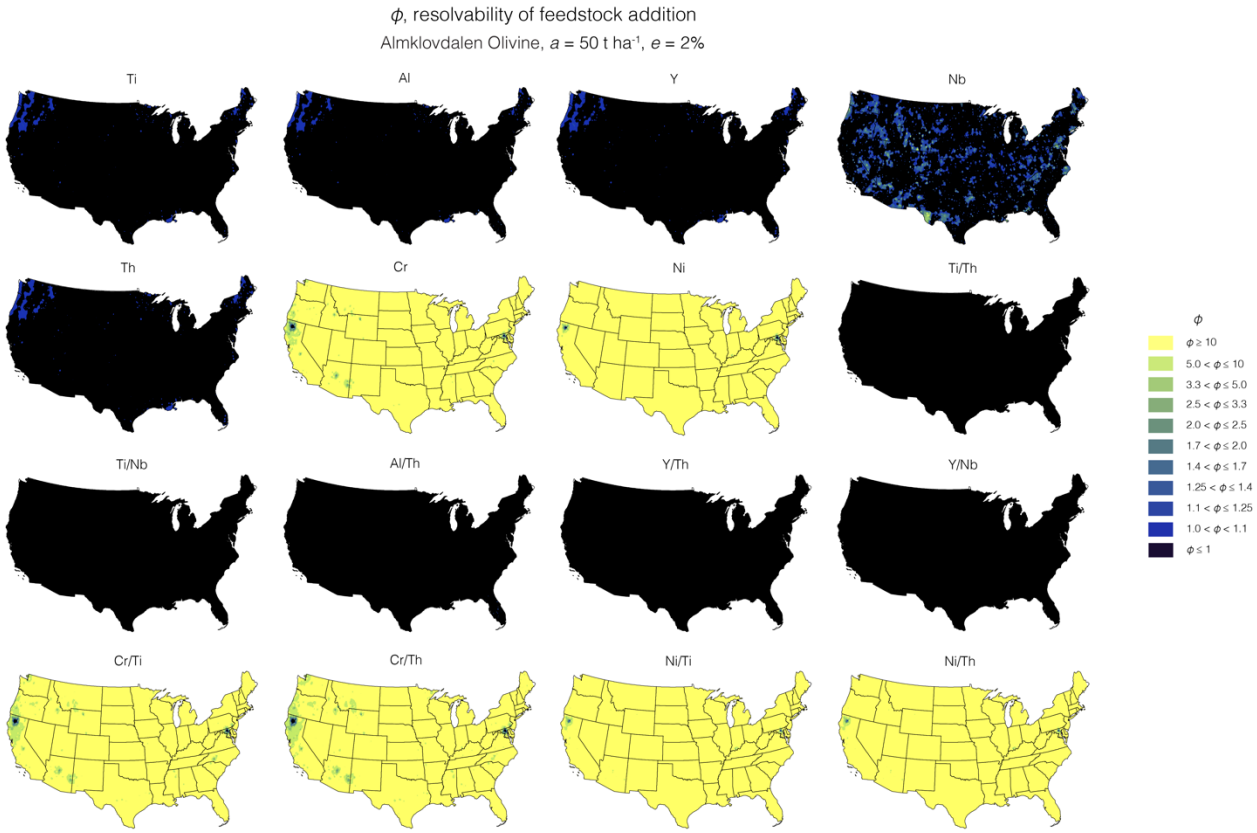

Figure S29: Comparison of the resolvability of feedstock addition (φ) for Almklovdalen Olivine based on different proxies of feedstock addition (i), assuming a = 50 t ha^{-1} and e = 2%.

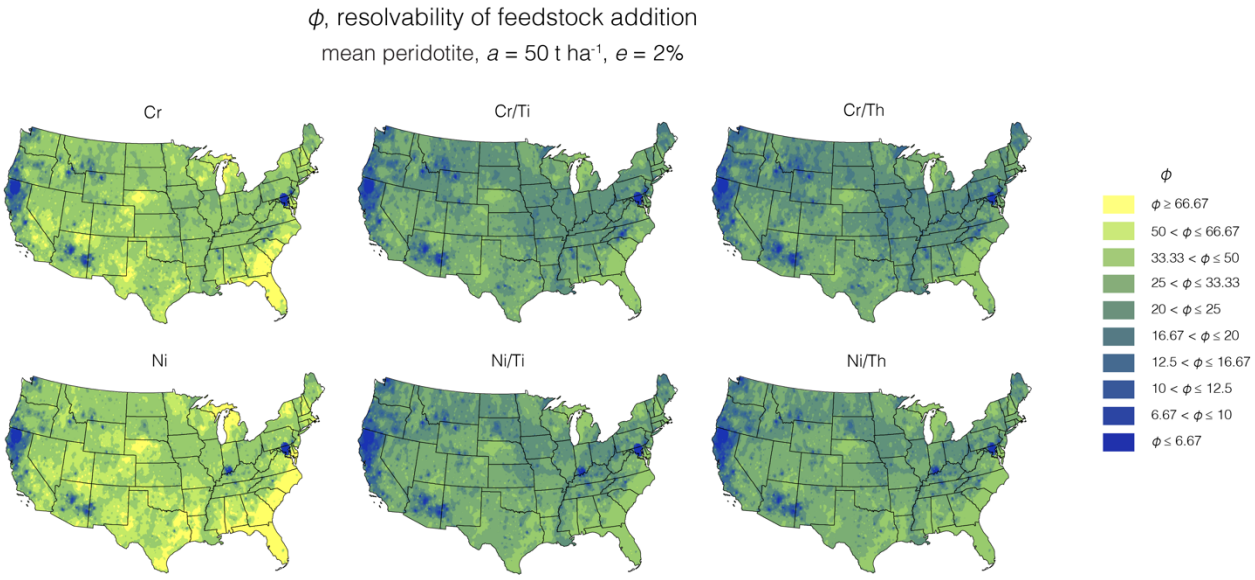

Figure S30: Comparison of the resolvability of feedstock addition (φ) for mean peridotite based on different proxies of feedstock addition (i), assuming a = 50 t ha^{-1} and e = 2%. The figure has a different color scale compared to Figure S28 to resolve variability for φ > 10. While φ values for Cr and Ni, as well as their ratios with Ti and Th, are promising, viability of these proxies depends on the ability to demonstrate immobility at the EW field site (see main text section 4.4).

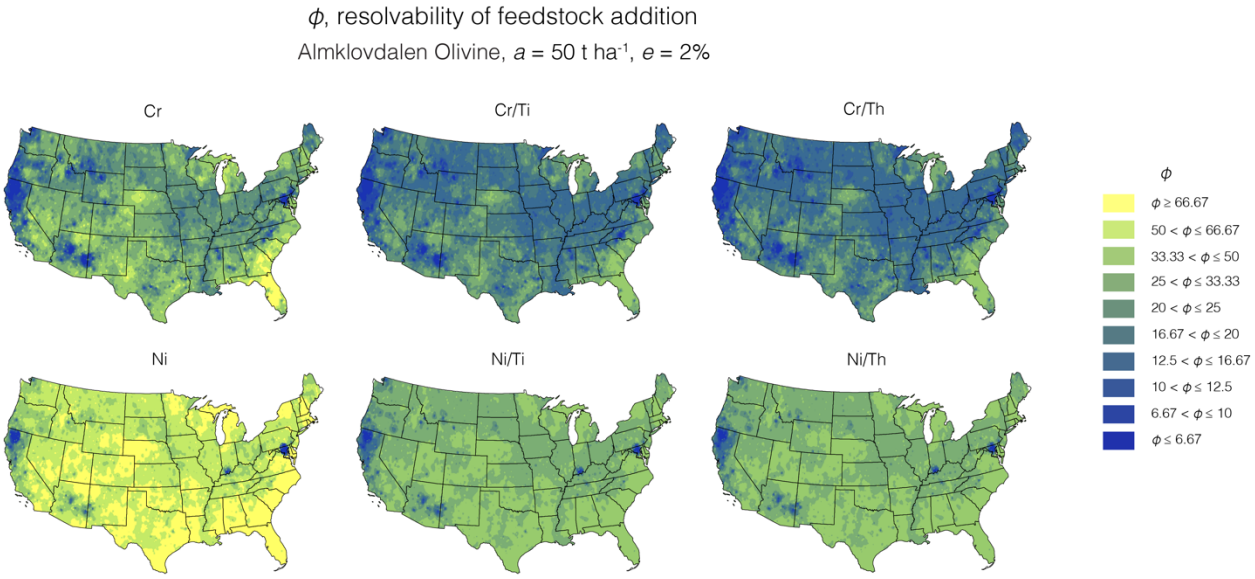

Figure S31: Comparison of the resolvability of feedstock addition (φ) for Almklovdalen Olivine based on different proxies of feedstock addition (i), assuming a = 50 t ha^{-1} and e = 2%. The figure has a different color scale compared to Figure S28 to resolve variability for φ > 10. While φ values for Cr and Ni, as well as their ratios with Ti and Th, are promising, viability of these proxies depends on the ability to demonstrate immobility at the EW field site (see main text section 4.4).

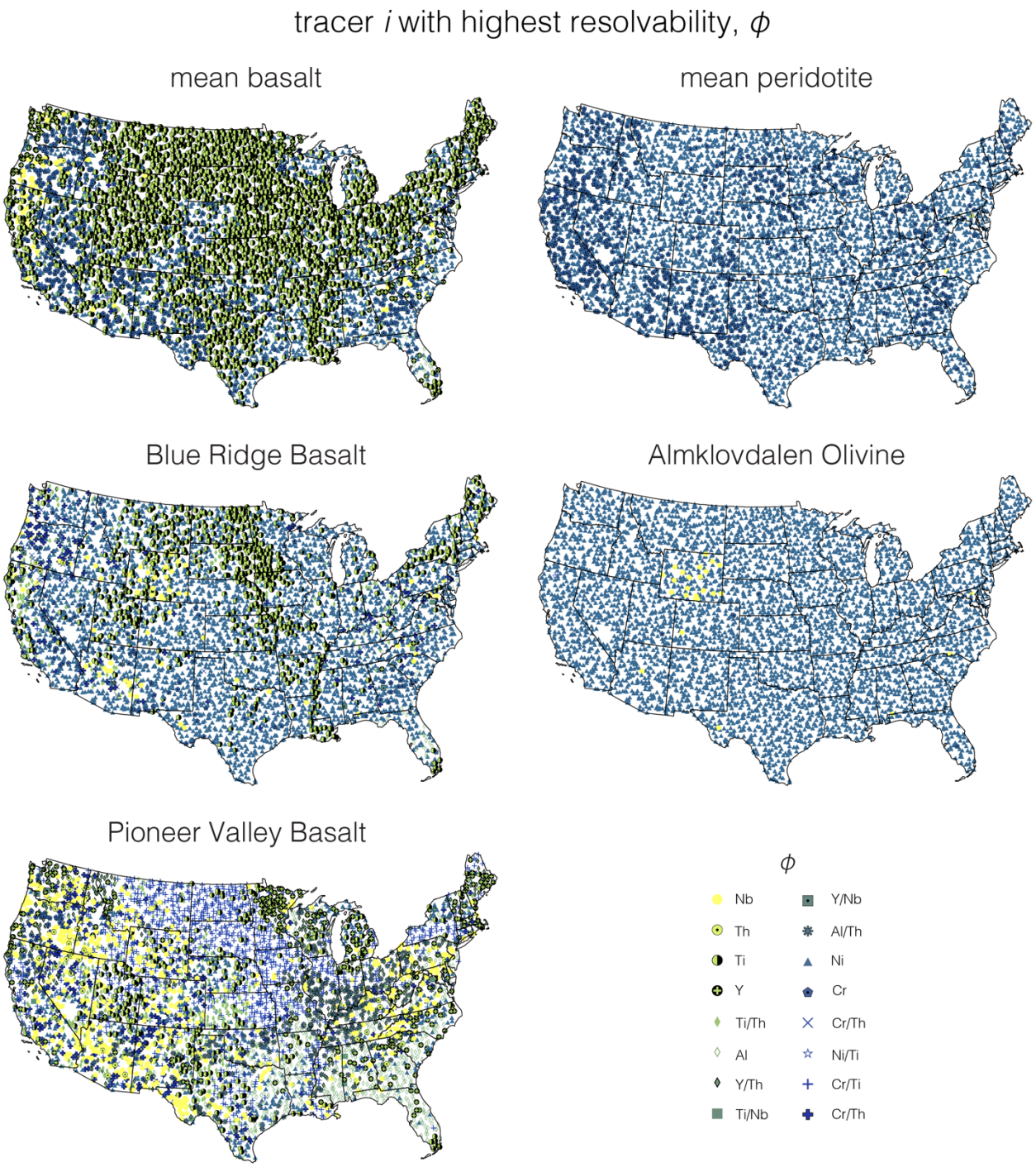

Figure S32: The immobile tracer i with the highest value of φ at each site contained in the USGS 'Geochemical and mineralogical data for soils of the conterminous United States' database. (Smith et al., 2013) for all feedstocks. See main text for a detailed analysis. Potential caveats for Ni and Cr in terms of mobility in the weathering zone are discussed in section **Error! Reference source not found.**.

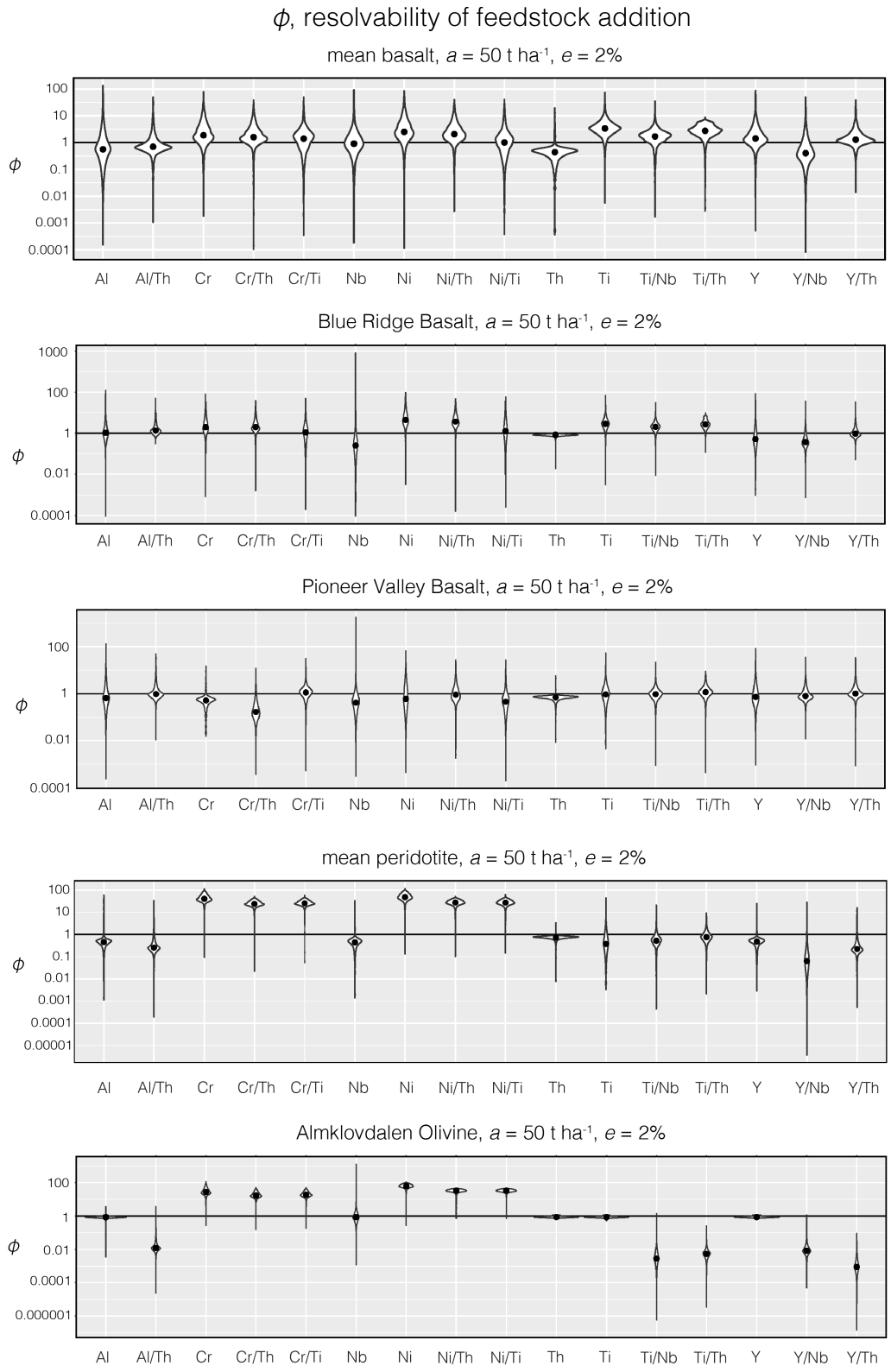

Figure S33: Violin plots for all feedstock addition proxies (i) for the five considered feedstocks assuming a = 50 t ha^{-1} and e = 2%. The best proxy for each data site is shown in Figure S34.

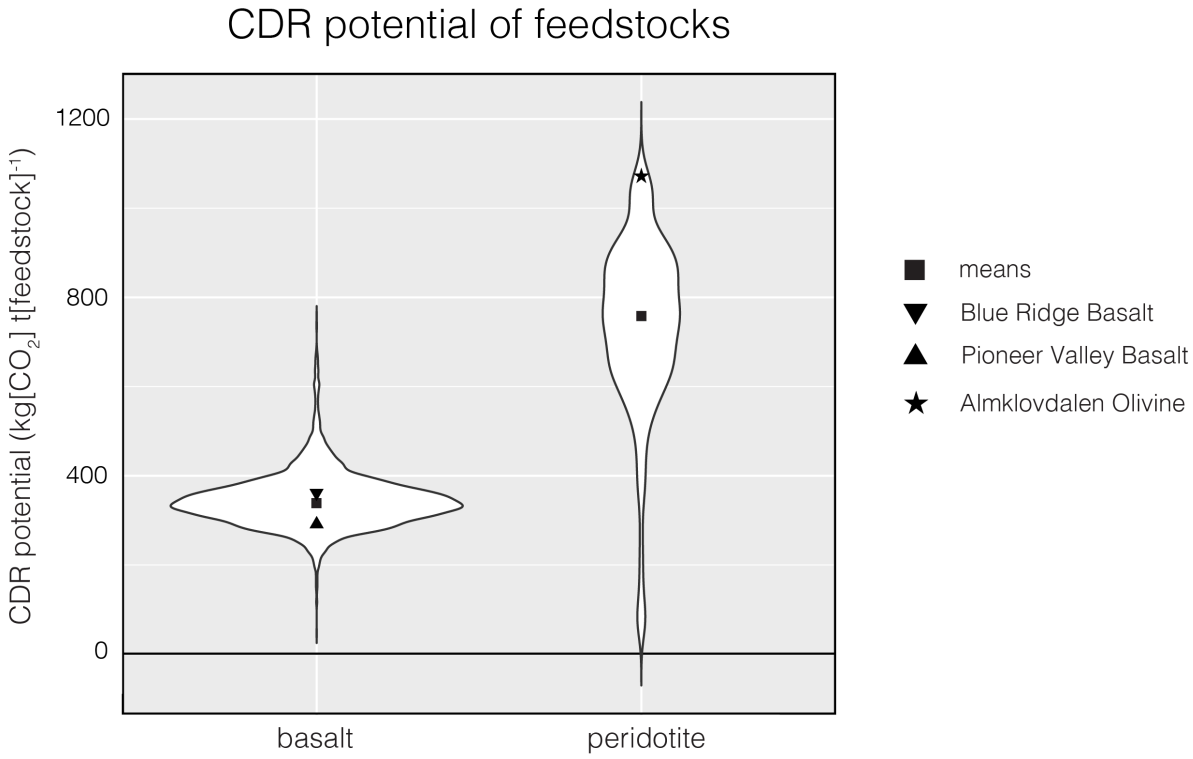

Figure S34: CDR potential for the basalts and peridotites contained in the GEOROC database (Lehnert et al., 2000). See main text for more details on the selection criteria of samples from the GEOROC database. The CDR potential was calculated using a modified Steinour equation (Renforth, 2012, 2019) – essentially this approach assumes that cations released from EW are charge balanced by bicarbonate ions. This calculation of CDR potential does not take any sort of downstream carbon leakage or emissions in the EW process into account.

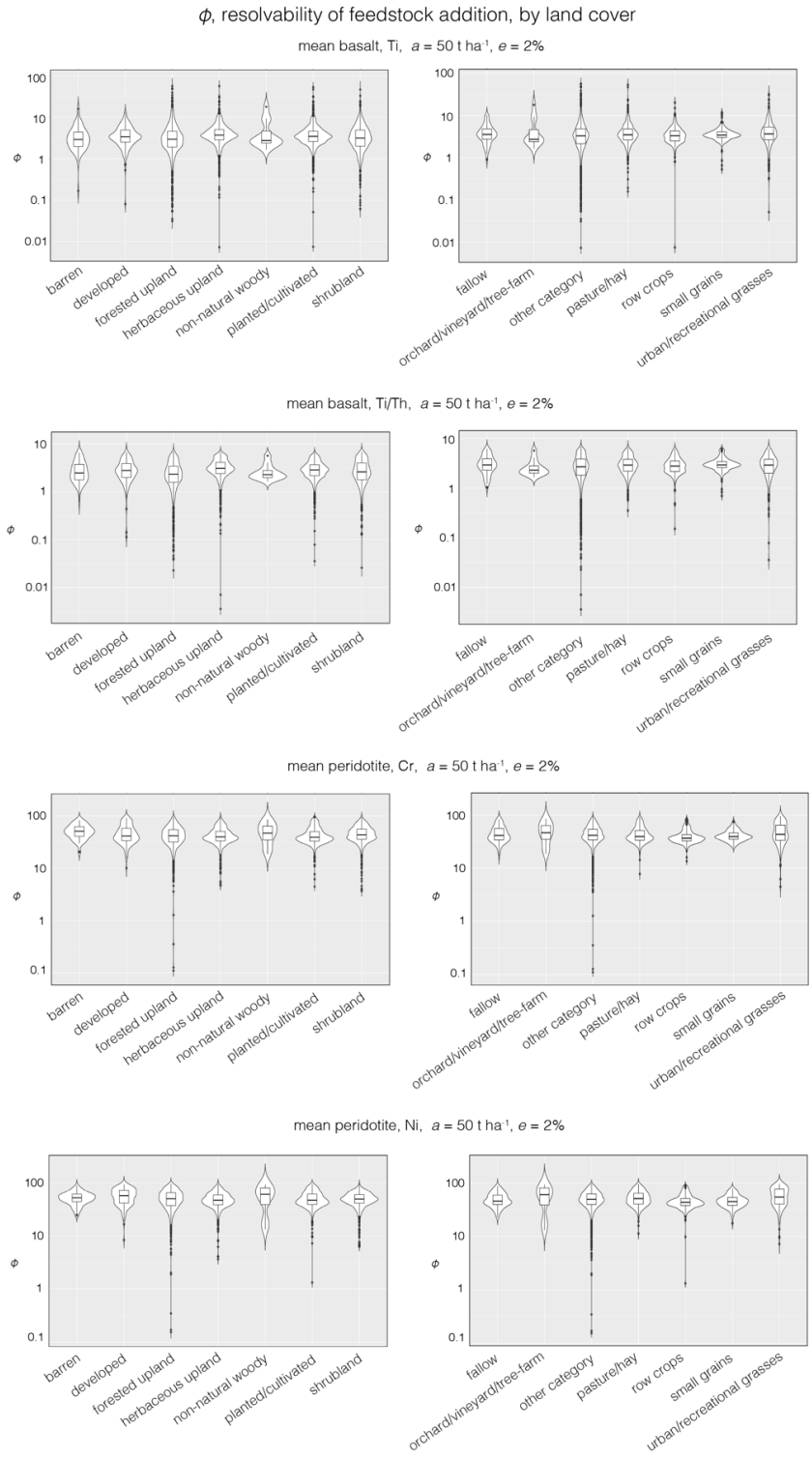

Figure S35: Violin and box plots of the resolvability of EW feedstock addition (φ) for i = Ti and Ti/Th for mean basalt, and i = Ni and Cr for mean peridotite. The data are grouped by relevant categories in the sections "Landcover1" (left) and "Landcover2" (right) columns of the USGS 'Geochemical and mineralogical data for soils of the conterminous United States' dataset (Smith et al., 2013).

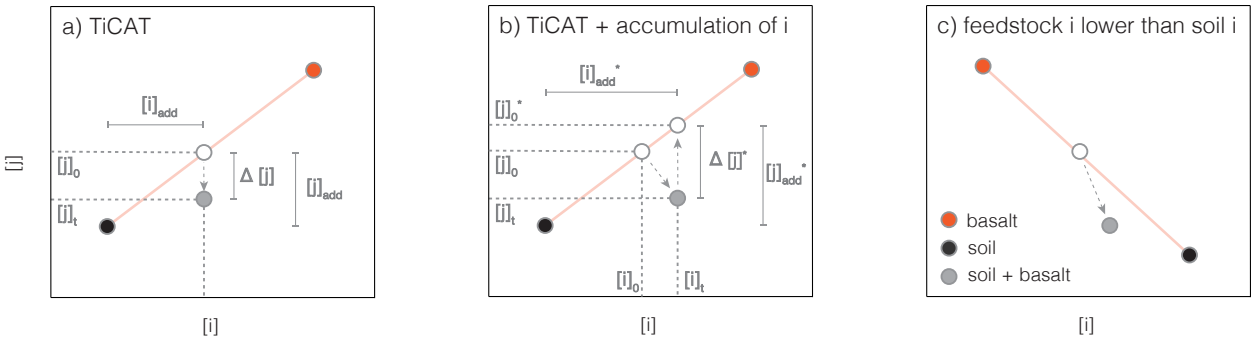

Figure S36: In the simplest formulation of soil-based mass-balances approaches, the addition of feedstock to soil samples is estimated from the concentration of an immobile element *i* in the soil+basalt mixture (when *i* in soil and feedstock endmembers is known; panel a). In this case, feedstock addition is estimated from the additional *i* in the soil+feedstock mix relative to the soil baseline. However, in reality, the dissolution of feedstock will cause an enrichment of *i* in the post-weathering soil+feedstock mix relative to its initial pre-weathering (post-application) composition, because while the immobile elements of the feedstock remain in the mix, the volume of the soil+feedstock mix decreases as feedstock dissolves (panel b). In panel b, *i* and *j* with a "*" superscript refer to apparent feedstock additions and resulting estimates of additions of *i* and *j*, which still need to be corrected for this enrichment process to yield true dissolution rates. A more detailed analysis of this processes can be found elsewhere (Reershemius & Suhrhoff, 2023; Reershemius & Kelland et al., 2023). The study presented here does not account for this process for two reasons; first, in the context of EW resolvability it increases the resolvability of EW signals because the post-weathering soil+feedstock data point falls further away from the mixing line. Not accounting for this in the framework here is conservative because it assumes the initial ($[i]_0$) concentration of *i*, which falls closer to the mixing line, providing a stricter criterion for resolvability. Second, for elements that are enriched in the feedstock – which are the focus of this study – this process can be corrected for accurately (Reershemius & Kelland et al., 2023). However, enrichment of immobile elements does have important consequences for feedstock-soil combinations where *i* concentrations are lower in the feedstock than in the soil. Here, the enrichment will cause the post-weathering soil+feedstock mix to fall closer or onto the mixing line defined by soil and feedstock endmembers (c). Hence, for these soil-feedstock combinations, not accounting for immobile element enrichment will overestimate resolvability. This is for example an issue when calculating φ for Almklovalen Olivine based on *i* = Ti (Figure S22). The apparent resolvability is a result of extremely low Ti concentrations in Almklovdalen Olivine. However, the process laid out in panel c (see also main text) prevents feedstock addition to actually be resolvable in this scenario. In general, the framework introduced here should only be applied to soil-feedstock combinations where *i* is larger in feedstock than soils. In these settings, the framework used here is appropriate and conservative. As a result, the online tools accompanying this paper does not compute calculation of φ values for soil-feedstock where *i* is smaller in feedstocks than soils to prevent erroneous overestimation of resolvability φ for unsuitable soil-feedstock combinations.

References used in the SI material

Bowen, H. J. M. (1979). *Environmental chemistry of the elements.* Academic Press.

Caspari, T., Bäumler, R., Norbu, C., Tshering, K., & Baillie, I. (2006). Geochemical investigation of soils developed in different lithologies in Bhutan, Eastern Himalayas. *Geoderma*, *136*(1–2), 436–458. https://doi.org/10.1016/j.geoderma.2006.04.017

Cheng, H., Hao, F., Ouyang, W., Liu, S., Chunye, L., & Wenjing, Y. (2012). Vertical distribution of rare earth elements in a wetland soil core from the Sanjiang Plain in China. *Journal of Rare Earths*, *30*(7), 731–738. https://doi.org/10.1016/S1002-0721(12)60120-3

Diatloff, E., Asher, C. J., & Smith, F. W. (1996). Concentrations of rare earth elements in some Australian soils. *Australian Journal of Soil Research*, *34*(5), 735–747. https://doi.org/10.1071/SR9960735

El-Ramady, H. (2010). *Ecotoxicology of rare earth elements: ecotoxicology of rare earth elements within soil and plant environments*. VDM Verlag Dr. Müller.

Fodor, M., Hegedüs, A., & Stefanovits-Bányai, É. (2005). Zirconium induced physiological alterations in wheat seedlings. *Biologia Plantarum*, *49*(4), 633–636. https://doi.org/10.1007/s10535-005-0065-y

Kabata-Pendias, A., & Pendias, H. (2003). *Trace elements in soils and plants*. CRC Press.

Laul, J. C., Weimer, W. C., & Rancitelli, L. A. (1979). Biogeochemical distribution of rare earths and other trace elements in plants and soils. *Physics and Chemistry of the Earth*, *11*(C), 819–827. https://doi.org/10.1016/0079-1946(79)90076-4

Lehnert, K., Su, Y., Langmuir, C. H., Sarbas, B., & Nohl, U. (2000). A global geochemical database structure for rocks. *Geochemistry, Geophysics, Geosystems*, *1*(5). https://doi.org/10.1029/1999gc000026

Li, X., Chen, Z., Chen, Z., & Zhang, Y. (2013). A human health risk assessment of rare earth elements in soil and vegetables from a mining area in Fujian Province, Southeast China. *Chemosphere*, *93*(6), 1240–1246. https://doi.org/10.1016/j.chemosphere.2013.06.085

Lijun W. et al. (2004). Biogeochemical cycle and residue of extraneous rare earth elements in agricultural ecosystem. *Journal of Rare Earth Elements*, *22*(5), 701–706.

Loell, M., Reiher, W., & Felix-Henningsen, P. (2011). Contents and bioavailability of rare earth elements in agricultural soils in Hesse (Germany). *Journal of Plant Nutrition and Soil Science*, *174*(4), 644–654. https://doi.org/10.1002/jpln.201000265

Markert, B. (1987). The pattern of distribution of lanthanide elements in soils and plants. *Phytochemistry*, *26*(12), 3167–3170. https://doi.org/10.1016/S0031-9422(00)82463-2

Markert, B., & De Li, Z. (1991). Natural background concentrations of rare-earth elements in a forest ecosystem. *Science of the Total Environment, The*, *103*(1), 27–35. https://doi.org/10.1016/0048-9697(91)90350-N

Marques, R., Prudêncio, M. I., Rocha, F., Cabral Pinto, M. M. S., Silva, M. M. V. G., & Ferreira da Silva, E. (2012). REE and other trace and major elements in the topsoil layer of Santiago island, Cape Verde. *Journal of African Earth Sciences*, *64*, 20–33. https://doi.org/10.1016/j.jafrearsci.2011.11.011

Miao, L., Xu, R., Ma, Y., Zhu, Z., Wang, J., Cai, R., & Chen, Y. (2008). Geochemistry and biogeochemistry of rare earth elements in a surface environment (soil and plant) in South China. *Environmental Geology*, *56*(2), 225–235. https://doi.org/10.1007/s00254-007-1157-0

Moreira, C. G. (2014). *Elementos terras raras em solos agrícolas com aplicações de fertilizante fosfatado e fosfogesso*. Thesis, Federal University of Lavras.

Öhlander, B., Land, M., Ingri, J., & Widerlund, A. (1996). Mobility of rare earth elements during weathering of till in northern Sweden. *Applied Geochemistry*, *11*(1–2), 93–99. https://doi.org/10.1016/0883-2927(95)00044-5

Oliveira, K. A. P., Menezes, M., Von Sperling, E., & Jacomino, V. M. F. (2012). Transfer factor of rare earth elements from phosphogypsum amended Brazilian tropical soils to lettuce, corn and soybean. *The Journal of Solid Waste Technology and Management*, *38*(3), 202–210. https://doi.org/10.5276/JSWTM.2012.202

Pais, I., & Jones Jr, J. B. (1997). *The handbook of trace elements*. Crc Press.

Ramos, S. J., Dinali, G. S., Oliveira, C., Martins, G. C., Moreira, C. G., Siqueira, J. O., & Guilherme, L. R. G. (2016). Rare Earth Elements in the Soil Environment. *Current Pollution Reports*, *2*(1), 28–50. https://doi.org/10.1007/s40726-016-0026-4

Reershemius, T., Kelland, M. E., Davis, I. R., D'Ascanio, R., Kalderon-Asael, B., Asael, D., Suhrhoff, T. J., Epihov, D. E., Beerling, D. J., Reinhard, C. T., & Planavsky, N. J. (2023). Initial Validation of a Soil-Based Mass-Balance Approach for Empirical Monitoring of Enhanced Rock Weathering Rates. *Environmental Science & Technology*. https://doi.org/10.1021/acs.est.3c03609

Reershemius, T., & Suhrhoff, T. J. (2023). On error, uncertainty, and assumptions in calculating carbon dioxide removal rates by enhanced rock weathering in Kantola et al ., 2023. *Global Change Biology*, *October*, 1–3. https://doi.org/10.1111/gcb.17025

Renforth, P. (2012). The potential of enhanced weathering in the UK. *International Journal of Greenhouse Gas Control*, *10*, 229–243. https://doi.org/10.1016/j.ijggc.2012.06.011

Renforth, P. (2019). The negative emission potential of alkaline materials. *Nature Communications*, 1–8. https://doi.org/10.1038/s41467-019-09475-5

Sadeghi, M., Morris, G. A., Carranza, E. J. M., Ladenberger, A., & Andersson, M. (2013). Rare earth element distribution and mineralization in Sweden: An application of principal component analysis to FOREGS soil geochemistry. *Journal of Geochemical Exploration*, *133*, 160–175. https://doi.org/10.1016/j.gexplo.2012.10.015

Salminen, R., Batista, M. J., Bidovec, M., Demetriades, A., De Vivo, B., De Vos, W., Duris, M., Gilucis, A., Gregorauskiene, V., Halamic, J., Heitzmann, P., Lima, A., Jordan, G., Klaver, G., Klein, P., Lis, J., Locutura, J., Marsina, K., Mazreku, A., O'Connor, P. J., … Tarvainen, T. (2005). FOREGS Geochemical Atlas of Europe , Part 1 : Background Information , Geochemical Atlas of Europe Part 2 Interpretation of Geochemical Maps , Additional Tables ,. In *EuroGeoSurveys* (Issue July 2014). Geological Survey of Finland.

Shahid, M., Ferrand, E., Schreck, E., & Dumat, C. (2013). Behavior and impact of zirconium in the soil-plant system: Plant uptake and phytotoxicity. *Reviews of Environmental Contamination and Toxicology*, *221*, 107–127. https://doi.org/10.1007/978-1-4614-4448-0_2

Smidt, G. A., Koschinsky, A., De Carvalho, L. M., Monserrat, J., & Schnug, E. (2011). Heavy metal concentrations in soils in the vicinity of a fertilizer factory in Southern Brazil. *Landbauforschung Volkenrode*, *61*(4), 353–364.

Smith, B., Rawlins, B. G., Cordeiro, M. J. A. R., Hutchins, M. G., Tiberindwa, J. V., Sserunjogi, L., & Tomkins, A. M. (2000). The bioaccessibility of essential and potentially toxic trace elements in tropical soils from Mukono district, Uganda. *Journal of the Geological Society*, *157*(4), 885–891. https://doi.org/10.1144/jgs.157.4.885

Smith, D. B., Cannon, W. F., Woodruff, L. G., Solano, F., Kilburn, J. E., & Fey, D. L. (2013). Geochemical and mineralogical data for soils of the conterminous United States. *U.S. Geological Survey Data Series*, *801*(April), 1–26. https://doi.org/10.3133/ds801

Takeda, A., Kimura, K., & Yamasaki, S. I. (2004). Analysis of 57 elements in Japanese soils, with special reference to soil group and agricultural use. *Geoderma*, *119*(3–4), 291–307. https://doi.org/10.1016/j.geoderma.2003.08.006

Tyler, G., & Olsson, T. (2002). Conditions related to solubility of rare and minor elements in forest soils. *Journal of Plant Nutrition and Soil Science*, *165*(5), 594–601. https://doi.org/10.1002/1522-2624(200210)165:5<594::AID-JPLN594>3.0.CO;2-K

Uchida, S., Tagami, K., & Hirai, I. (2007). Soil-to-plant transfer factors of stable elements and naturally occurring radionuclides (1) upland field crops collected in japan. *Journal of Nuclear Science and Technology*, *44*(4), 628–640. https://doi.org/10.1080/18811248.2007.9711851

Yoshida, S., Muramatsu, Y., Tagami, K., & Uchida, S. (1998). Concentrations of lanthanide elements, Th, and U in 77 Japanese surface soils. *Environment International*, *24*(3), 275–286. https://doi.org/10.1016/S0160-4120(98)00006-3

Zhang, Q., Lei, T., & Zhao, J. (2008). Estimation of the detachment rate in eroding rills in flume experiments using an REE tracing method. *Geoderma*, *147*(1–2), 8–15. https://doi.org/10.1016/j.geoderma.2008.07.002